Investigation of the flow inside an urban canopy immersed into an atmospheric boundary layer using laser Doppler anemometry

Sophie Herpin[1,2,3] · Laurent Perret[1,4] · Romain Mathis[5] · Christian Tanguy[6] · Jean-Jacques Lasserre[6]

Abstract
Laser Doppler anemometry (LDA) is used to investigate the flow inside an idealized urban canopy consisting of a staggered array of cubes with a 25% density immersed into an atmospheric boundary layer with a Reynolds number of $\delta^+ = 32{,}300$. The boundary layer thickness to cube height ratio ($\delta/h = 22.7$) is large enough to be representative of atmospheric surface layer in neutral conditions. The LDA measurements give access to pointwise time-resolved data at several positions inside the canopy ($z = h/4$, $h/2$, and h). Synchronized hot-wire measurements above the canopy (inertial region and roughness sublayer) are also realized to get access to interactions between the different flow regions. The wall-normal mean velocity profile and Reynolds stresses show a good agreement with available data in the literature, although some differences are observed on the standard deviation of the spanwise component. A detailed spectral and integral time scale analysis inside the canopy is then carried out. No clear footprint of a periodic vortex shedding on the sides of the cubes could be identified on the power spectra, owing to the multiple cube-to-cube interactions occuring within a canopy with a building density in the wake interference regime. Results also suggest that interactions between the most energetics scales of the boundary layer and those related to the cube canopy take place, leading to a broadening of the energy peak in the spectra within the canopy. This is confirmed by the analysis of coherence results between the flow inside and above the canopy. It is shown that linear interactions mechanisms are significant, but reduced compared to smooth-wall boundary-layer flow. To our knowledge, this is the first time such results are shown on the dynamics of the flow inside an urban canopy.

1 Introduction

Understanding atmospheric flows in urban areas is of primary importance in the context of urban densification of the worldwide population. From a purely aerodynamic point of view, the flow inside an urban canopy can be seen as the flow developing around three-dimensional obstacles immersed into a high Reynolds number, rough boundary layer flow (the atmospheric surface layer), with complex interactions. A first statistical picture of the flow was provided by Macdonald et al. (2000), but its dynamics has never been fully addressed.

Despite the very large range of building size, shape, or spatial arrangement in real-life built areas, the simplified canopy consisting of a regular array of cubes is now widely accepted as a canonical representation. Several contributions investigating the turbulent flow around a single wall-mounted cube can be found in the literature, and are a good starting point to understand the dynamics inside such a canopy. In these studies, the cube is usually large meaning that its dimension h is of the same order or larger than

✉ Sophie Herpin
sophie.herpin@agrocampus-ouest.fr

[1] Laboratoire de recherche en Hydrodynamique, Energétique et Environnement Atmosphérique (LHEEA UMR CNRS 6598) Ecole Centrale de Nantes, B.P. 92101, 44321 Nantes Cedex 3, France

[2] Laboratoire de mécanique de Lille (LML)-Ecole Centrale de Lille, Université Lille I- Sciences et technologies, CNRS: FRE3723, Arts et Métiers ParisTech-Bâtiment M6 Bvd Paul Langevin, 59655 Villeneuve D Ascq Cedex, France

[3] Present Address: AGROCAMPUS Ouest, 2 Rue André Le Nôtre, 49045 Angers Cedex, France

[4] Institut de Recherche en Sciences et en Technologies de la Ville (IRSTV)-FR CNRS 2488-Ecole Centrale de Nantes Rue Massenet, 81931 44319 Nantes Cedex 3, France

[5] Institut de Mécanique des Fluides de Toulouse, IMFT, Université de Toulouse, CNRS, Toulouse, France

[6] DANTEC Dynamics SAS, 8 Rue Gutenberg ZI de la Butte, 91620 Nozay, France

the boundary layer thickness δ. Using flow visualizations, Martinuzzi and Tropea (1993) proposed a very comprehensive representation of the flow around a single wall-mounted cube (Fig. 1). The incoming flow is deviated by the presence of the cube, with spanwise and vertical by-pass motions. The sharp edges of the cube induce a flow separation, together with vortex shedding on the sides and top of the cube. Close to the wall, in the upstream stagnation region of the cube, a large horseshoe vortex is formed. In the downstream region of the cube, a second attached horseshoe vortex is formed, followed by an elongated recirculation region. The flow around a tandem of two cubes with variable separation length S in the streamwise and/or spanwise directions was investigated by Sakamoto and Haniu (1988) and Martinuzzi and Havel (2004). Different regimes of vortex shedding and Strouhal numbers could be identified depending on the ratio S / h. Meinders and Hanjalic (1999) realized a study with an array of large cubes. Due to the low surface density (6.25%) of the canopy, many common features were found with the single cube flow. Although vortex shedding on top of the cubes occured over a broader range of frequencies, a Strouhal number of 0.1 could still be identified through a peak in the power spectral density of the vertical velocity component.

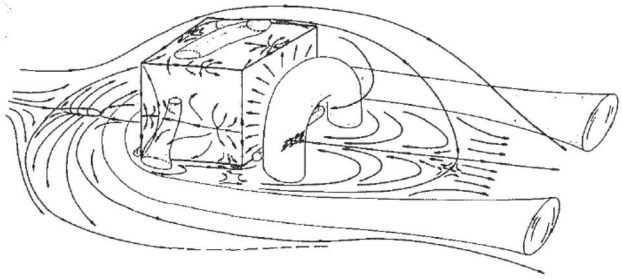

Fig. 1 Schematic representation of the flow around a single mounted cube, from Martinuzzi and Tropea (1993)

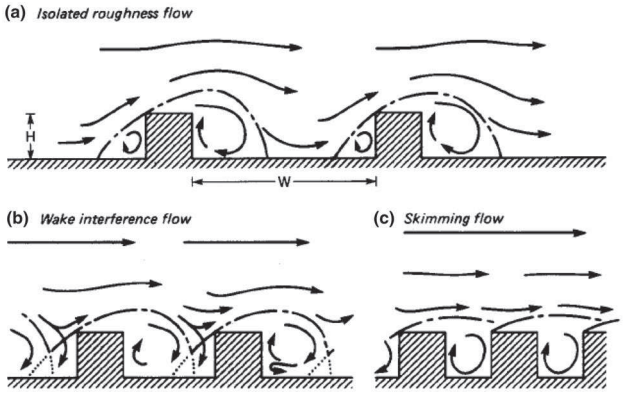

Fig. 2 The three flow regimes in an array of cubes from Oke (1988)

For atmospheric flows over buildings, the cube dimension h becomes small compared to the boundary layer thickness δ. The effect of the ratio δ/h was investigated by Castro and Robins (1977) in the range [0.1, 10]. For thick boundary layers such that $\delta/h \geq 1.4$, the vortex shedding activity was suppressed due to the effect of increased upstream turbulence. In the case of urban canopies, represented by array of multiple cubes, the flow becomes even more complex. Oke (1988) and Grimmond and Oke (1999) identified three flow regimes depending on the packing area density of the urban roughness (see Fig. 2): the isolated roughness flow in which the organisation of the flow is very similar to single-cube flow, the wake interference flow, and the skimming flow.

For the last two regimes, the tight clearance and high complexity of the flow makes measurements within the canopy extremely challenging, which may explain the relatively low number of studies found in the literature. For instance, hot-wire anemometry is not possible, due to the intrusivity of the probe in this confined environment, and to the three-dimensionality of the flow. Laser-based techniques are the only viable solution to perform measurements in the canopy. Full field measurement techniques such as particle image velocimetry (PIV) give access to spatial information, and allow to investigate the spatial organization as well as length scale of the flow. On the other hand, laser Doppler anemometry provide time-resolution of the flow dynamics, at the cost of point-wise measurements.

The first insights into the dynamics of the flow over dense urban canopies have been given by Castro et al. (2006), using hot-wire anemometry (HWA) and laser Doppler anemometry (LDA) to measure the flow above and below the canopy interface respectively. They investigated a staggered array with a 25% density pertaining to the wake-interference regime, with $\delta/h = 7.4$ and $\delta^+ = \delta u_*/\nu \approx 980$ (where u_* is the friction velocity and ν the kinematic viscosity). Particularly, they defined four measurement positions around the cube chosen to be representative of the cube array pattern (see Fig. 4): P0 centred on top of the cube (not shown here), P1 located downstream of the cube, P2 positioned upstream and P3 at the middle of a streamwise alley. An inflection point was found at about $z = h/2$ on the mean velocity profile, which is consistent with the presence of an horseshoe vortex. On the Reynolds stresses, a maximum was found near the canopy top, especially at point P1 in connection with the shear layer separating from the top leading edge of the cube. Two-point correlations and power spectral density analysis were carried out, but restricted to the roughness sublayer and therefore time scales, length scales, or structure angles were not given inside the canopy.

Following these first successful measurements, and to retrieve spatial information within the canopy, Castro's group made use of both PIV and LDA in a staggered-cube 25% canopy with $\delta/h = 13.5$ with $\delta^+ \approx 430$ (Reynolds and

Castro 2008). The LDA measurements were performed at consistent locations with their previous study. The 2D-2C PIV was realized in a streamwise/wall-normal x–z plane centred on a streamwise row of cubes, and going down to the wall. Due the limitation on the visual access imposed by the canopy, the streamwise extent of the measurements realized below the canopy roof was restricted to $1h$ downstream and $1h$ upstream of the cube, covering the area comprising points P1 and P2, but not point P3. The mean statistics of the flow were extracted and showed a very good agreement between PIV and LDA. A detailed two-point spatial correlation and quadrant analysis was then undertaken using PIV data. In contrast to smooth-wall data, it was found that sweeps are dominant close the wall within the canopy region. Outside the canopy, the events become more similar to smooth-wall boundary layer, with a larger part of ejection events. The auto-correlation of the streamwise velocity component near the canopy top ($z/h = 1.2$) is analyzed, and a two-scale behaviour is evidenced with two integral scales valid for both P1 and P2: $L_x/h = 0.8$ for small streamwise separations and $L_x/h = 3$ at larger separations.

On the numerical side, Coceal et al. (2006) performed an obstacle-resolving DNS of a turbulent boundary layer over 25% canopies (with staggered, aligned, and square spatial arrangements), and carried out an analysis of the mean velocity and the turbulent stresses. A good agreement was found with the experimental data of Castro et al. (2006). It was also found that, for a given density, these statistics depend significantly on the cube pattern. In a subsequent study based on their DNS data with the staggered 25% canopy, Coceal et al. (2007) investigated the coherent structures inside the logarithmic region above the roughness.

Some limitations arise from the above-mentioned studies: the datasets are obtained at moderate Reynolds number ($h^+ = hu_*/\nu \in [430;1080]$) as well as small boundary layer thickness (δ) to cube height (h) ratio (7.4–13.5). This is due to the limited thickness of the boundary layer in conventional wind-tunnels, or to CPU limitations for DNS. This does not enable a faithful reproduction of the very large scale motions in the outer region of real atmospheric flows, and therefore of the complex inner/outer interactions with the canopy flow.

Atmospheric wind-tunnels or in situ facilities enable to achieve a better representation of real atmospheric flows. In Rivet (2014) and Blackman and Perret (2016), an atmospheric wind-tunnel was used to investigate urban canopies with a 25% dense staggered array of cubes. The cube Reynolds number was typically $h^+ = 1420$ and the ratio $\delta/h = 22.7$. These studies were dedicated to the analysis of the inner/outer interaction between the boundary layer flow and the canopy. In both studies, stereoscopic PIV (SPIV) measurements were realised in a $x-z$ plane and gave access to spatial information in the inertial layer, roughness sublayer, and to a portion of the canopy flow [in the vicinity of the canopy roof for Rivet (2014), and in the downstream region of a cube for Blackman and Perret (2016)]. In Rivet (2014), a detailed spatial correlation analysis was undertaken, and a two-scale behaviour was also evidenced on the R_{uu} correlation at the canopy interface and in the roughness sublayer. In Blackman and Perret (2016), a skewness decomposition analysis revealed an amplitude modulation mechanism of the small scales by the large scales, as previously reported in smooth wall-bounded flows (Mathis et al. 2009). Blackman et al. (2017) completed this analysis by performing a detailed analysis of the kinetic turbulent energy budget within both the canopy and the roughness sublayer, showing the link between coherent structures and energy transfers in these regions.

In situ experiments have been carried out by Inagaki and Kanda (2008) on a 25% aligned array canopy at 1:5 geometric scale using the Comprehensive Outdoor Scale Model (COSMO) facility, in cross-wind neutral conditions. Pointwise measurements were realized using five sonic anemometers located at heights of $4h$, $3h$, $2h$, $1.5h$ and $1h$ from the ground, covering the roughness sub-layer and part of the inertial layer. Power spectra on the streamwise, spanwise, and wall-normal velocities (S_u, S_v, S_w, respectively) as well as the co-spectra S_{uw} are analyzed and compared with spectra obtained in flat rural areas by Kaimal et al. (1972). In inner scaling (u_* for the velocity and U/z for the frequency), the spectra are found to be quite close to the reference spectra from Kaimal et al. (1972) in the high-wave number range. In contrast, large difference appear in the low frequency domain for S_u and S_v where a secondary peak clearly emerge for the urban canopy. Inagaki and Kanda (2008) associate this low frequency peak with inactive motions originating from outer layer disturbances, with a characteristics length scale given by the boundary layer thickness δ rather than the distance to the wall. The peak of energy on the spectra at the canopy interface $z = h$ are found to be shifted towards higher frequency, this shift being attributed to the wake production from the cubes. The wall-normal evolution of the peak frequency on the three velocity components is finally analyzed and compared with full-scale cities.

Overall, all experimental studies dedicated to urban canopies have mainly focused their analysis on the canopy interface and the region above (roughness and inertial layer), or given a partial view of the canopy. Being the central place of human activity, a good knowledge of the flow inside the urban canopy, in conditions that are representative of real-life environments, is very important for urban management considerations (air quality, pedestrian comfort). Reference experimental data in this flow region are also of interest for numerical modelers, as full resolution of atmospheric flow in urban environment is out of reach given today computational resources. In the present contribution, we focus our attention on the flow within a 25% density array of staggered cubes immersed into

a thick turbulent boundary layer generated in the atmospheric wind-tunnel of Ecole Centrale de Nantes. The boundary layer is representative of the atmospheric surface layer in neutral conditions at the scale 1:200. The flow benefit from a high Reynolds number ($h^+ = 1420$ and $\delta^+ = 32300$) and a ratio $\delta/h = 22.7$ which is relevant for real urban-like environments. Time-resolved laser Doppler anemometry measurements are carried out at three heights inside the canopy ($z = h/4, h/2, h$) at positions consistent with Castro's work (P1, P2, P3) as well as extra points located in the vicinity of a cube.

The main objectives of the paper are:

- to assess a new experimental database dedicated to the canopy region, where relatively little material can be found in the literature,
- to study the spatial distribution of energy within the canopy,
- and to analyze the dynamics of the flow around the cube, including the characteristics time scales of the canopy flow, the characteristic frequencies of the main peak of energy, and the linear interactions mechanisms with the roughness sublayer and inertial region above the canopy.

For that purpose, a detailed spectral and auto-correlation analysis is carried out. Great care is taken in qualifying the LDA dataset, its quality and its limitation. To give more perspective on the results, these are compared, when possible, to that of other urban canopy results available in the literature.

2 Experimental design and methods

2.1 Experimental setup

Experiments have been performed in the LHEEA atmospheric wind-tunnel at Ecole Centrale de Nantes. The wind tunnel has a 5:1 inlet ratio contraction and a free-stream turbulence intensity within the empty wind tunnel of 0.5% with spanwise uniformity to within ± 5% (Savory et al. 2013). After appropriate conditioning with five vertical spires and a fence, the atmospheric surface layer develops over a 24 m long floor, fully covered with an urban canopy model consisting of a regular, staggered array of $h = 50$ mm high, sharp-edge cubes with a packing area density of 25% (see Fig. 3). The main characteristics of the flow are summarized in Table 1. Following Cheng and Castro (2002), the friction velocity u_* was estimated from measurements of the form drag of a cube instrumented with 36 pressure taps on both the leeward and windward face. The displacement height d was also estimated from these measurements following its definition provided by Jackson (1981) which states that d is the height at which the drag of the canopy is exerted and, therefore, can be calculated from the moment of the drag about the transverse axis at the base of the obstacle. The roughness length was estimated from the fit of the meteorological form of the log law $\langle u \rangle / u_* = 1/\kappa \log((z-d)/z_0)$, with $\kappa = 0.4$ (Cheng and Castro 2002). The normalized friction velocity u_*/U_e has been found independent from the Reynolds number in the investigated range $32000 < \delta^+ < 50000$. This, combined to the rather high value of the Reynolds number $h^+ = 1420$ confirm that the flow is in fully rough regime. The boundary layer thickness δ is defined here as the height where the mean velocity is equal to 99% of the free-stream velocity. More details on the facility, the characteristics of the turbulent boundary layer flow, as well as on the estimation of the friction velocity, displacement thickness and aerodynamic roughness length can be found in Rivet (2014) and Perret et al. (2017).

The dynamics of the flow inside the canopy was recorded using a two-component laser Doppler anemometry system from Dantec Dynamics (model FlowExplorer DPSS), operating in backward scattering mode. The LDA probe is equipped with a 300 mm focal length, and the measurement volume is illuminated using two lasers emitting at 532 and 561 nm with a maximum power of 300 mW. A schematic representation of the experimental setup is shown in Fig. 3. In this study, the streamwise, spanwise and wall-normal directions are denoted x, y, z, respectively and associated with velocity components u, v, w. The probe is positioned below the wind-tunnel floor and oriented vertically. The floor of the wind-tunnel is equipped with a transparent window to ensure optical access to the flow inside the canopy. This configuration enables the measurement of the streamwise u and spanwise v velocity components inside the canopy. The measurement volume size is $\Delta_x = \Delta_y = 0.1$ mm and $\Delta_z = 1$ mm, or in wall units $\Delta_x^+ = \Delta_y^+ = 2.8$ and $\Delta_z^+ = 28$, or as a fraction of the cube height $\Delta_x/h = \Delta_y/h = 0.002$ and $\Delta_z/h = 0.02$

Seven streamwise/spanwise positions around the cube have been chosen to be representative of the canopy pattern: P1, P2, P3 as defined by Castro's group (Castro et al. 2006; Reynolds and Castro 2008), plus three additional points A, B, C, D to study the flow dynamics in the vicinity of a cube (see Fig. 4). Depending on the point location,

Table 1 Main characteristics of the flow; z_0 is the aerodynamic roughness length and d is the displacement thickness

U_e (m/s)	δ (m)	u_* (m/s)	δ/h	u_*/Ue	δ^+	h^+	z_0/h	d/h
5.78	1.134	0.4278	22.7	0.074	32300	1420	0.11	0.59

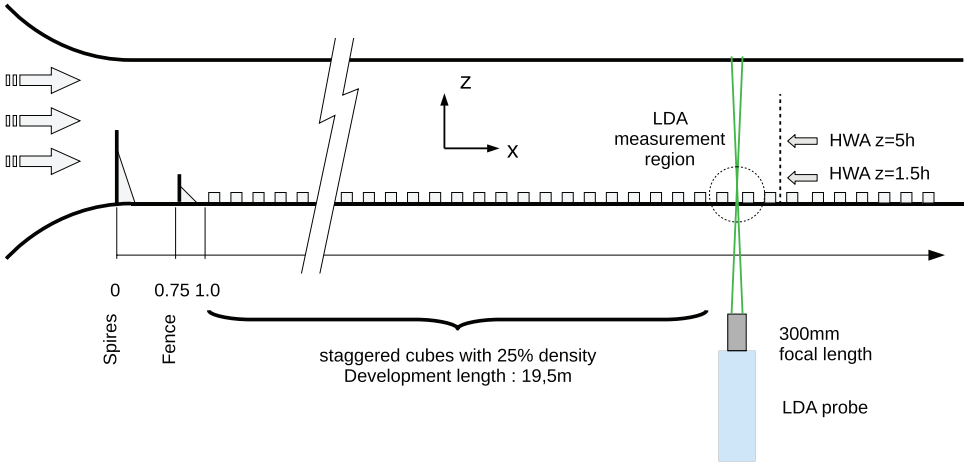

Fig. 3 Schematic representation of the LHEEA atmospheric wind-tunnel and LDA and HWA measurement setup

one to three wall-normal positions have been scrutinised at altitudes $z = 0.25h$, $0.5h$ and $1h$. To validate the LDA data against available data obtained from hot-wire anemometry and particle image velocimetry, three additional wall-normal positions have been measured above the canopy ($z = 1.25h$, $1.45h$ and $5h$) at point noted E. A summarise of the measured points is given in Table 2.

The mean LDA particle rate $\dot{N}_{\mathrm{LDA}}$ depends on the position of the measurement point. The raw mean particle rate increased with the distance to the wall and typically varied between 150 and 1300 Hz inside the canopy and up to 1617 Hz above the canopy. After acquisition, inter-arrival time of particles were computed on the raw data inside and above the canopy. Particles with an inter-arrival time lower than $\Delta t_{\mathrm{min}} = \Delta_x / u_{\mathrm{mean},z}$ (where Δ_x is the streamwise extent of the measurement volume and $u_{\mathrm{mean},z}$ is the mean streamwise velocity at height z) have overlapping residence time inside the LDA measurement volume, or are counted twice. This may lead to an incorrect evaluation of the Doppler burst, and contribute to measurement noise. Therefore, these particles were removed from the final dataset. A subsequent outliers detection was performed on both velocity components and points such that $|(u_i - \bar{u}_i)| > \sigma_{u_i}(5 + S_{u_i})$ were removed (where σ_{u_i} and S_{u_i} are the variance and skewness of the velocity component u_i). The skewness of the velocity distribution was included to take into account non-normal PDF distribution in the canopy (typically observed on the streamwise velocity at the canopy interface, $z = h$). In any case the percentage of outliers detected was very low, under 0.1%. The effective mean data rate obtained for each measurement point is shown in Table 3, the lowest data rate being 99 Hz and the largest 1546 Hz. The duration of the LDA acquisition is also reported in Table 3: the LDA signal was acquired over 1200 s (20 min) for each point at $z = h/4$ and over 3600 s (1 h) for each point at $z = h/2$, h, $1.25h$, $1.45h$, $5h$. These data rates and acquisition times should be compared with the main frequencies (and the inverse quantity, the turn-over time) in the flow that can be estimated using the flow main parameters: U_e and δ for the outer flow and u_* and h for the flow inside the canopy. The results are shown in Table 4. The LDA data rates are thus between 1 and 2 order of magnitude higher than the expected characteristics frequencies of the flow, which ensures an appropriate time resolution of the flow dynamics. Depending on the point

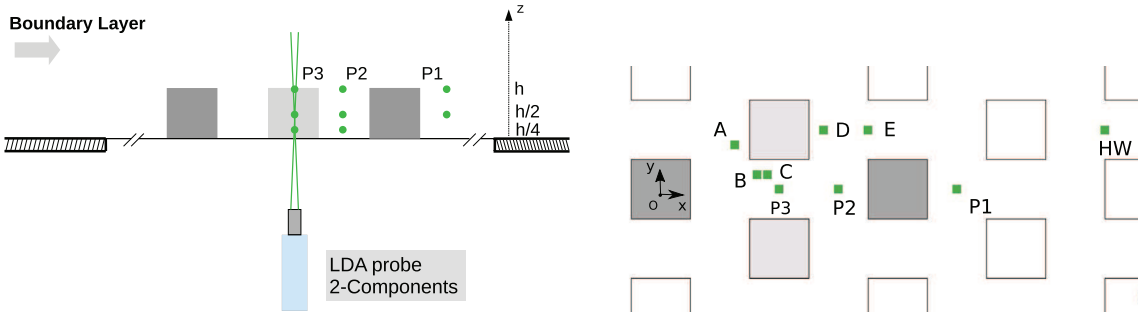

(a) side view **(b)** top view

Fig. 4 Position of the LDA measurement points inside the canopy **a** side view **b** top view

Table 2 Position of LDA measurement points

Flow region	LDA point	x/h	y/h	z/h					
				1/4	1/2	1	1.25	1.45	5
upstream of a cube	P2	3	0	X	X	X			
	A	1.25	0.75		X	X			
middle of a streamwise alley	P3	2	0	X	X	X			
corner of a cube	B	1.625	0.25	X	X	X			
	C	1.8	0.25		X	X			
downstream of a cube	P1	5	0		X	X			
	D	2.75	1			X			
	E	3.5	1				X	X	X

The origin of the coordinate system for x and y is set at the center of the upstream cube in dark-grey color, as shown in Fig. 4b, and $z = 0$ at the wall. The canopy pattern has a $4h$ periodicity in **x** direction, a $2h$ periodicity in **y** direction, and a $(2h \cdot \mathbf{x}, 1h \cdot \mathbf{y})$ periodicity in diagonal

location, the acquisition time is comprised between 6000 and 30,000 turn-over times in outer scaling (respectively, 10,000–18,000 turn-over times in inner scaling). These very long acquisition times were chosen to reach good statistical convergence of high-order quantities. Both data rate and sampling time allow us to converge small to large scales content.

In order to get access to the interactions between the surface layer flow and the canopy flow, hot-wire measurements of the streamwise velocity in the roughness sub-layer at $z = 1.5h$ and in the inertial layer at $z = 5h$ were synchronized with the LDA measurements in the canopy. Two single-wire probes were placed at an equivalent position to point E, but shifted $4h$ downstream to avoid any blockage effect on the LDA measurements. The wire has a diameter of 5 µm, and a length of 1.25 mm. This length is comparable with the height of the LDA measurement volume, resulting in a similar spatial resolution. The hot-wire probes were operated in the constant temperature mode. The signals were passed through a suitable analog low-pass filter to prevent aliasing, and then digitalized and acquired at a sampling frequency of 10 kHz. A TTL measurement running signal was emitted by the LDA system and was recorded with the HWA data acquisition system to enable synchronisation of the datasets. In addition to this acquisition at 10 kHz, the hot-wire analog signal was also fed as an analog input to the LDA system and sampled at the LDA frequency.

2.2 Algorithms to estimate power spectral density from LDA data

The computation of power spectral density (PSD) with LDA data is not trivial, because the LDA irregular sampling do not allow the use of standard Fast Fourier Transform (FFT) algorithms. Various methods have been reviewed in Benedict et al. (2000). A preliminary study was conducted on present data to compare several algorithms, including basic interpolation schemes, the refined Sample and Hold with correction from Nobach et al. (1998), the fuzzy Slotting algorithm from Van Maanen et al. (1999), or the arrival time quantization from Nobach (2016), taking the hot-wire spectrum at $z = 1.5h$ and $z = 5h$ as reference. Based on this preliminary study, it was decided to use the Refined Sample and Hold Algorithm from Nobach et al. (1998) for the analysis of our database. Indeed, this algorithm seems to provide the best trade-off between faithfulness, CPU efficiency, and low variance. The algorithm consists of the following steps:

Table 3 Mean effective data rate for each LDA point

LDA point	z/h	$\dot{N}_{LDA}$: mean datarate (Hz)	Acquisition time (s)
B	1/4	168	
P2	1/4	115	137	1200
P3	1/4	129	
A	1/2	144	
B	1/2	99	
C	1/2	148	175	3600
P1	1/2	337	
P2	1/2	232	
P3	1/2	223	
A	1	1048	
B	1	700	
C	1	246	453	3600
D	1	131	
P1	1	549	
P2	1	478	
P3	1	548	
E	1.25	370	370	3600
E	1.45	890	890	3600
E	5	1546	1546	3600

Table 4 Characteristic frequencies and turn-over times in the wind-tunnel flow in the outer- and inner-regions

f_{outer} (Hz)	f_{inner} (Hz)	t_{outer} (s)	t_{inner} (s)
5.1	8.6	0.2	0.12

– A zeroth order interpolation of the original LDA signal using a Sample and Hold scheme.
– Re-sampling at fixed frequency.
– Computation of the auto-correlation.
– Refinement of the auto-correlation with a correction to compensate the effect of the interpolation transfer function.
– FFT of the refined auto-correlation to get the PSD.

The Python library available on the signal and data processing Nambis website from Nobach and co-workers (http://ldvproc.nambis.de/index.html) was used for implementation.

A new extension of the original sample and hold algorithm is proposed to minimize the effect of measurement noise on the LDA power spectra. If we assume that the measurement noise of LDA is white, then it affects all frequencies of the power spectra. In contrast, in the temporal domain, the auto-correlation function is only affected at 0 time lag, where the noise correlates with itself, inducing an over-estimation of $R_{u_i u_i}(0)$:

$$R_{u_i u_i}(0) = \sigma_{ui}^2 + \epsilon_i^2 \tag{1}$$

This influence of noise can be classically visualized on the auto-correlation function by a sharp peak at $R_{u_i u_i}(0)$. To reduce the contamination of the power spectra by noise, it is possible to correct $R_{u_i u_i}(0)$ using an extrapolation from neighbouring points, before applying the Fourier transform. After careful inspection of the shape of auto-correlation function in the neighbourhood of $R_{u_i u_i}(0)$, the extrapolation function is chosen as the osculating parabola of the auto-correlation function for $z \geq h$, and as a decreasing exponential for $z < h$ (depending on the temporal resolution of the auto-correlation). The LDA spectrum using the refined Sample and Hold algorithm, with and without $R_{u_i u_i}(0)$ noise correction, is validated with the reference HWA spectrum at 10 kHz in the roughness sublayer and inertial layer. The results are shown in Fig. 5. As it can be seen, the inertial range is successfully resolved by LDA with both algorithm. The correction of $R_{u_i u_i}(0)$ reduces the bias induced by noise at high frequencies and gives further access to part of the dissipative range.

3 Results

3.1 Flow field in wall-parallel planes

To get a comprehensive view of the flow, a vector plot of the mean velocity and maps of standard deviation are provided for the three measured heights in the canopy, respectively, in Figs. 6 and 7. It should be noted that the measured points have been duplicated to fulfill the pattern and obtain a global overview. These maps allow us to visualize the data at all measurements points, including A, B, C, D, for which no data in the literature is available to compare with. Data are scaled using the friction velocity u_*. All obtained values are of this order, indicating that it is an appropriate scaling for the mean and fluctuating flow inside the canopy. It was also checked that the mean spanwise velocity component $\langle v \rangle$ is zero at points P1, P2, P3, as expected due to the symmetry of the flow. It should be noted that the spanwise velocity at $z = h/2$ for point P3 (visible on the map of standard deviation in Fig. 7) was not correctly measured, and will thus not be analyzed.

The effect of the wall-roughness is clearly visible through a deceleration of the fluid with decreasing wall-normal distance in the canopy. At the canopy interface, the mean flow is mostly longitudinal and rather uniform except for the sheltered region downstream of the cube (D and P1), which exhibits a significant velocity deficit. The fluctuations are important, quite uniform and isotropic, with a turbulence intensity about 50% of the average velocity. At the canopy mid-height, the presence of the obstacles induces a spanwise by-pass motion and an acceleration of the flow at the corner and in-between cubes (B, C, P3). The sheltering effect of the cube is strengthened, with a possible recirculation upstream of P1. At the corner (B) and downstream of the cube (P1), the flow has quite large spanwise fluctuations, which can indicate either the occurrence of vortical events or an intermittent meandering motion of the flow in diagonal alleys of the canopy. Finally, close to the wall (h / 4), a stagnation region is visible upstream of the cube (P2).

The covariance $\langle u'v' \rangle$ was also investigated, but not reported here. It has zero values as expected for symmetry reasons at points P1, P2, P3 on the LDA data. At the canopy top, the covariance is very weak throughout the $x - y$ plane. The largest magnitude is obtained at point B at $z = h/2$ (with $| < u'v' > | = 0.7 \times u_*^2$) and $z = h/4$ (with $| < u'v' > | = 0.6 \times u_*^2$), in connection with the activity of the shear layer separating from the side edges of the cube.

3.2 Wall-normal profiles at P1, P2, P3

The LDA mean velocity and standard deviation were computed using a Transit-Time weighting average scheme, to compensate the bias of the LDA technique towards higher-velocities (McKeon et al. 2007). The wall-normal profiles of $\langle u \rangle$, u_{RMS} and v_{RMS} at points P1, P2, P3, in inner scaling (i.e u_* for the velocity and h for the altitude z) are shown in Fig. 9 for the present LDA dataset in the canopy (blue color), and HW dataset in the outer flow (red color). As noted above, the spanwise velocity at $z = h/2$ for point P3 is not correctly measured by the LDA system and this point is then not shown in the figure (bottom row). LDA results obtained at point E above the canopy (at $z = 1.25h$ and $z = 1.45h$)

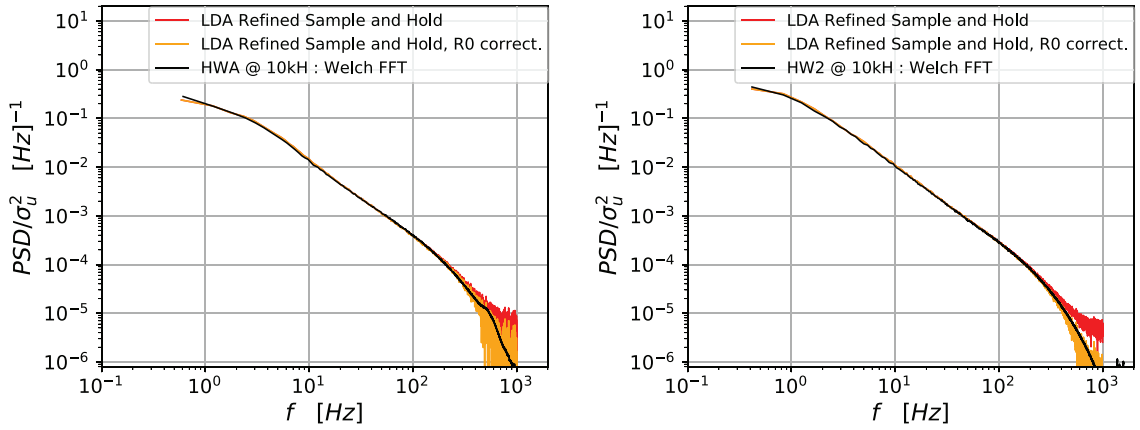

(a) $z = 1.5h$ ($\dot{N}_{LDA} = 890$Hz) **(b)** $z = 5h$ ($\dot{N}_{LDA} = 1546$Hz)

Fig. 5 Comparison of the power spectral density of streamwise velocity component obtained from HWA at 10 kHz and a standard FFT algorithm, with the PSD from LDA and a refined sample and Hold algorithm (re-sampling frequency at 2 kHz), with and without noise correction on R[0]. A block size of $12\delta/Ue$ and of $8.5\delta/Ue$ were used for the spectra at $z = 5h$ and $z = 1.5h$ respectively

are added for reference in each figure. The results are compared with the literature using other datasets with the same wall-roughness pattern (staggered array of cubes with a 25% density):

- datasets from the literature: LDA data of Castro et al. (2006) with $\delta/h = 7.4$ and $h^+ = 840$ and the DNS data of Coceal et al. (2007) with $\delta/h = 8$ and $h^+ = 500$ (grey and black color, respectively)
- datatsets from the author's group measured in the same facility as present data, and in the same conditions ($\delta/h = 22.7$ and $h^+ = 1420$) with PIV in a streamwise/wall-normal symmetry plane (green color): The data from Blackman and Perret (2016) give access to measurements over almost the full height of the canopy (down to $z/h = 0.1$), but only in the downstream region of a cube (the streamwise extent of the PIV plane $1h$); on the other hand, the data from Rivet (2014) give access to the full longitudinal extent of a streamwise alley ($3h$), but only in the upper part of the canopy (down to $z/h = 0.8$).

To facilitate the analysis of the results, the spatial resolution of the datasets $\max(\Delta_{x,y,z})$ (defined as the maximum length of the measurement volume or sensor, e.g., maximum dimension of the cell size for the DNS data, of the measurement volume for the LDA data, of the interrogation window for the PIV data, or the wire length for the hot-wire probe) are reported in Fig. 8, normalized with the cube height h. As it can be seen the spatial resolution of present LDA is the sharpest among all datasets considered. The averaging volume of the PIV from Rivet (2014) and Blackman and Perret (2016) is about four times larger. Averaging effects of the PIV are therefore expected on the velocity fluctuations.

The LDA data present an overall good collapse with PIV, DNS and HWA data on the u velocity component. The LDA data from Castro is also in good agreement, but exhibits a slight over-estimation compared to other datasets, as already spotted by Coceal et al. (2007). There is no details in Castro et al. (2006) about the use or not of a specific weighting scheme.

Above the canopy, the results from three different measurement techniques, namely PIV, HWA and LDA realized in the same facility and flow conditions can be compared. The three techniques are in excellent agreement for $\langle u \rangle$ and u_{RMS} at $z = 1.25h$ and $z = 1.45h$, which confirms the ability of the LDA system to measure faithfully and with a low level of noise the streamwise velocity component. Inside the canopy, the HWA technique is not feasable, and our LDA results can only be compared in the same flow conditions to the PIV results from Blackman and Perret (2016) at P1, and to the results from Rivet (2014) near the canopy interface. A very good agreement is noted on $\langle u \rangle$, while the PIV technique seem to underestimate by about 10–15% the peak of u_{RMS} at the canopy interface. On a different note, there is a large discrepancy between the PIV and the LDA data on the spanwise velocity component, with an estimation of v_{RMS} by the PIV which is systematically 30% lower than the LDA data throughout the canopy height. Again, this can be attributed to the averaging effect of PIV, accentuated on this velocity component by the fact that the spanwise velocity corresponds to the out-of-plane velocity in the PIV setup and thus to the reconstructed one in the stereoscopic configuration. Alternatively, this could also be due to experimental noise on this velocity component in the LDA data.

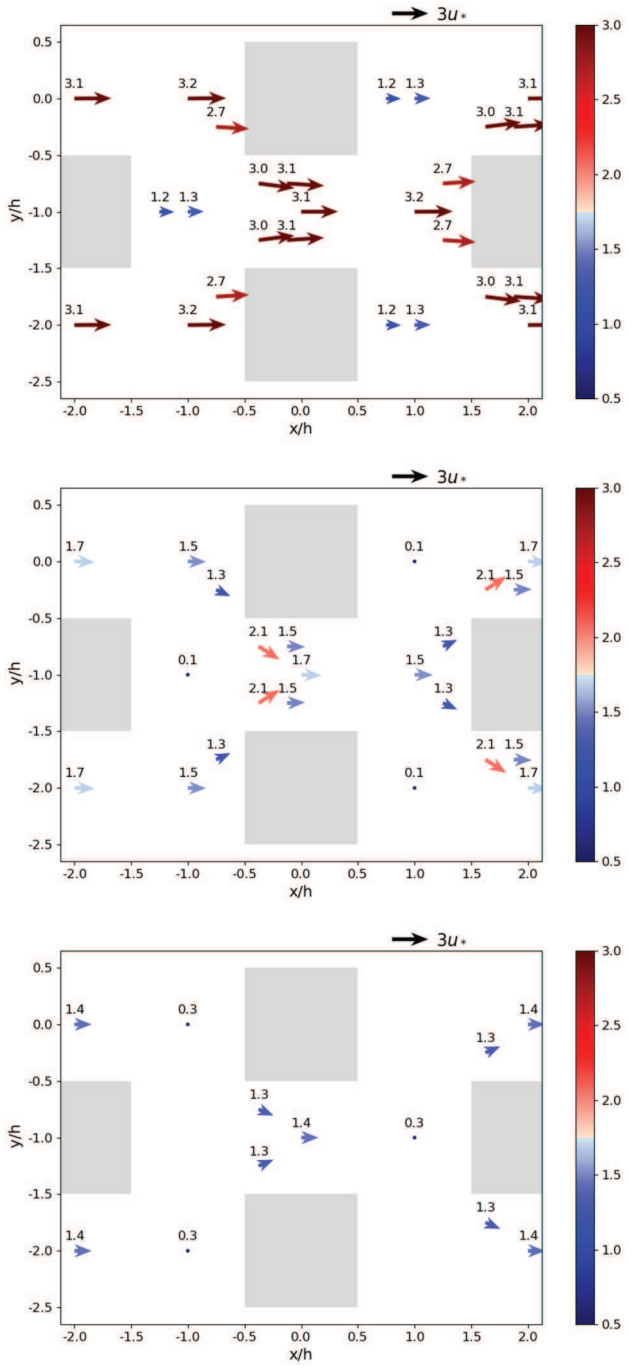

Fig. 6 Mean velocity field $\langle \mathbf{U} \rangle / u_*$ in wall-parallel planes inside the canopy at various heights: $z = h$ (top), $z = h/2$ (middle), $z = h/4$ (bottom), obtained with LDA data. The numerical values correspond to the velocity magnitude, non-dimensionalized with u_*. The measured point P1, P2, P3, A, B, C and D have been duplicated to fulfill the pattern

Looking now at the data from the literature, our LDA results are overall in good agreement with the LDA results from Castro et al. (2006) for $\langle u \rangle$, u_{RMS}, and even v_{RMS}. This means that there is a real difference on the estimation of the spanwise velocity component between the PIV technique on one side (Blackman and Perret 2016; Rivet 2014) and the LDA technique on the other side (present results and Castro et al. 2006). Unfortunately, the DNS results from Coceal et al. (2007) are not available on this velocity component, but there is a good agreement with present data on the streamwise velocity component. The good agreement of present data with the data from the literature, obtained at different flow conditions (in terms of δ^+, h^+, and δ/h), confirms that the inner scaling with u_* and h is appropriate from the canopy flow.

From a qualitative point of view, some features of the urban canopy flow mentioned in Sect. 1 can be retrieved and confirmed from the analysis of the wall-normal profiles of $\langle u \rangle$, u_{RMS} and v_{RMS}:

- Above the canopy ($z \geq 1.2h$), the flow within each dataset is spatially homogeneous, and there is no difference between the results at P1, P2, and P3.
- Inside the canopy, the flow is spatially heterogeneous: this is a fundamental difference between urban canopies and plant canopies,
- At the canopy interface, all measurement regions show an inflection point of the mean velocity profile, but the strength of the velocity gradient associated to that inflection point vary from one measurement station to another. In particular, the strongest gradient of both $\langle u \rangle$ and u_{RMS} is observed in the downstream region of a cube (P1), where the flow pattern is quite similar to a mixing layer flow pattern observed in plant canopies (Finnigan 2000), as suggested by Castro et al. (2006).
- In the region downstream of a cube (P1), and below the canopy interface, there is a strong sheltering effect of the cube, with $\langle u \rangle \approx 0$ for $0.3 \leq z/h \leq 0.8$.
- In the region upstream of a cube (P2), the profile of $\langle u \rangle$ shows two additional inflection points, at $z/h = 0.4$ and at $z/h = 0.1$ which is consistent with the presence of an upstream horseshoe vortex observed in the single-cube flow. A recirculation region with negative velocity is visible close to the wall. This wall-normal profile is in full agreement with the streamwise/wall-normal mean velocity field extracted through the middle of a cube by Coceal et al. (2006).
- At all points, a peak of streamwise velocity fluctuations u_{RMS} is visible at the canopy interface. This is less visible on the v-component, and seems dependent of the measurement technique, particularly at points P2 and P3 where no peak is visible on PIV results.

Finally, it should be noted that, unlike plant canopies, the flow inside urban canopies shows a strong spatial heterogeneity. In particular, the strength of the velocity gradient associated to the inflection point at the canopy interface is not

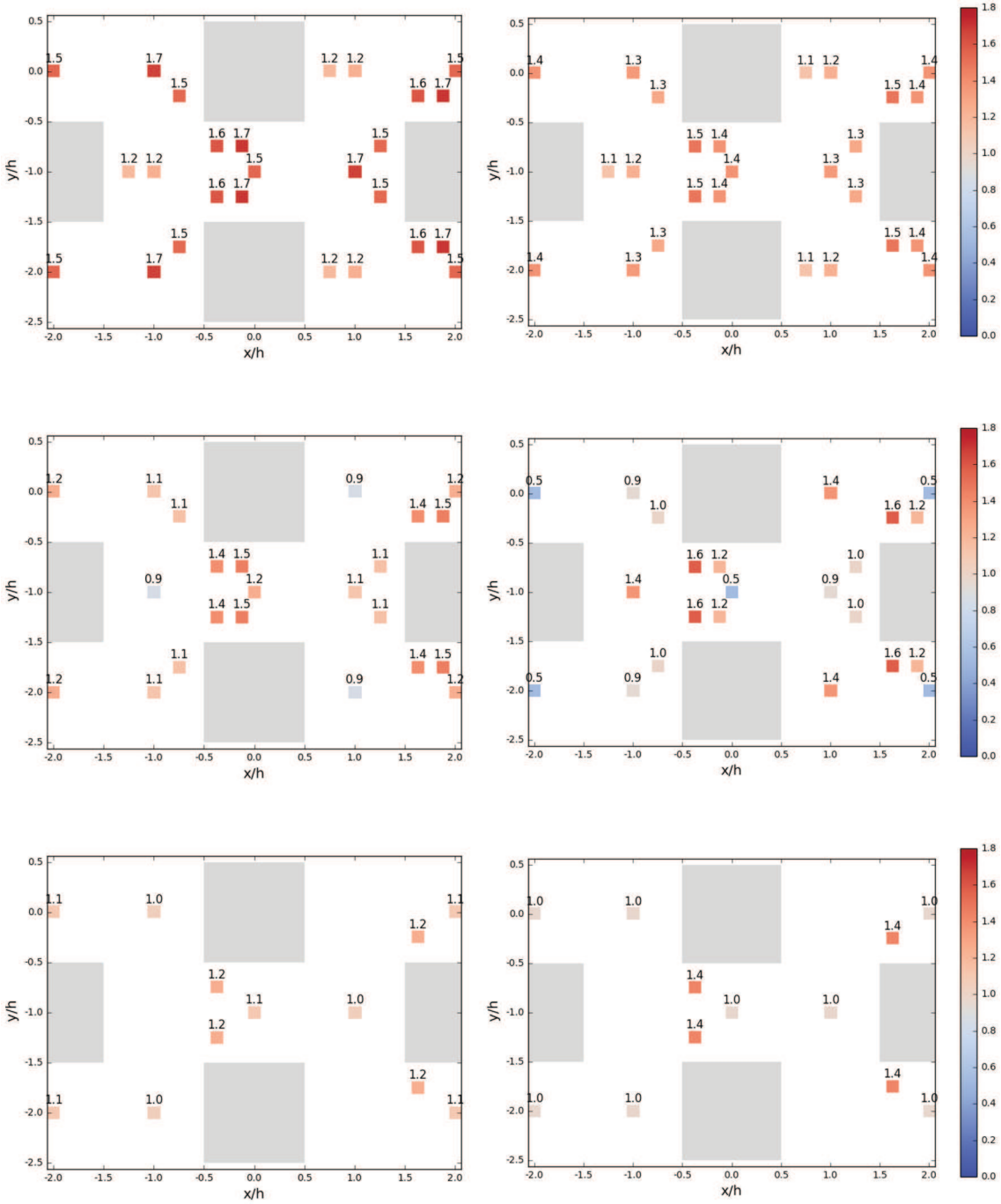

Fig. 7 Maps of standard deviation of streamwise velocity u_{RMS}/u_* (left column) and standard deviation of spanwise velocity v_{RMS}/u_* (right column) in wall-parallel planes inside the canopy at various heights: $z = h$ (top), $z = h/2$ (middle), $z = h/4$ (bottom), obtained with LDA data. The measured point P1, P2, P3, A, B, C and D have been duplicated to fulfill the pattern

uniform, and, deeper inside the canopy, secondary inflection points appear at some measurement locations. This make it difficult to derive models of the average mean velocity profile or to draw a general behavior of urban canopies based on results from one specific geometry. In order to overcome this issue, the next section is dedicated to spectral analysis of the flow around the cube to study prevalent scales and mechanisms that can be useful in term of modelling.

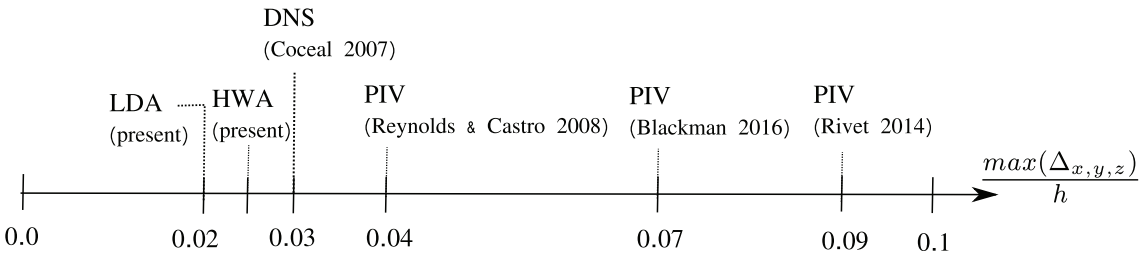

Fig. 8 Spatial resolution of the present datasets and available datasets from the literature, normalized with the cube height h

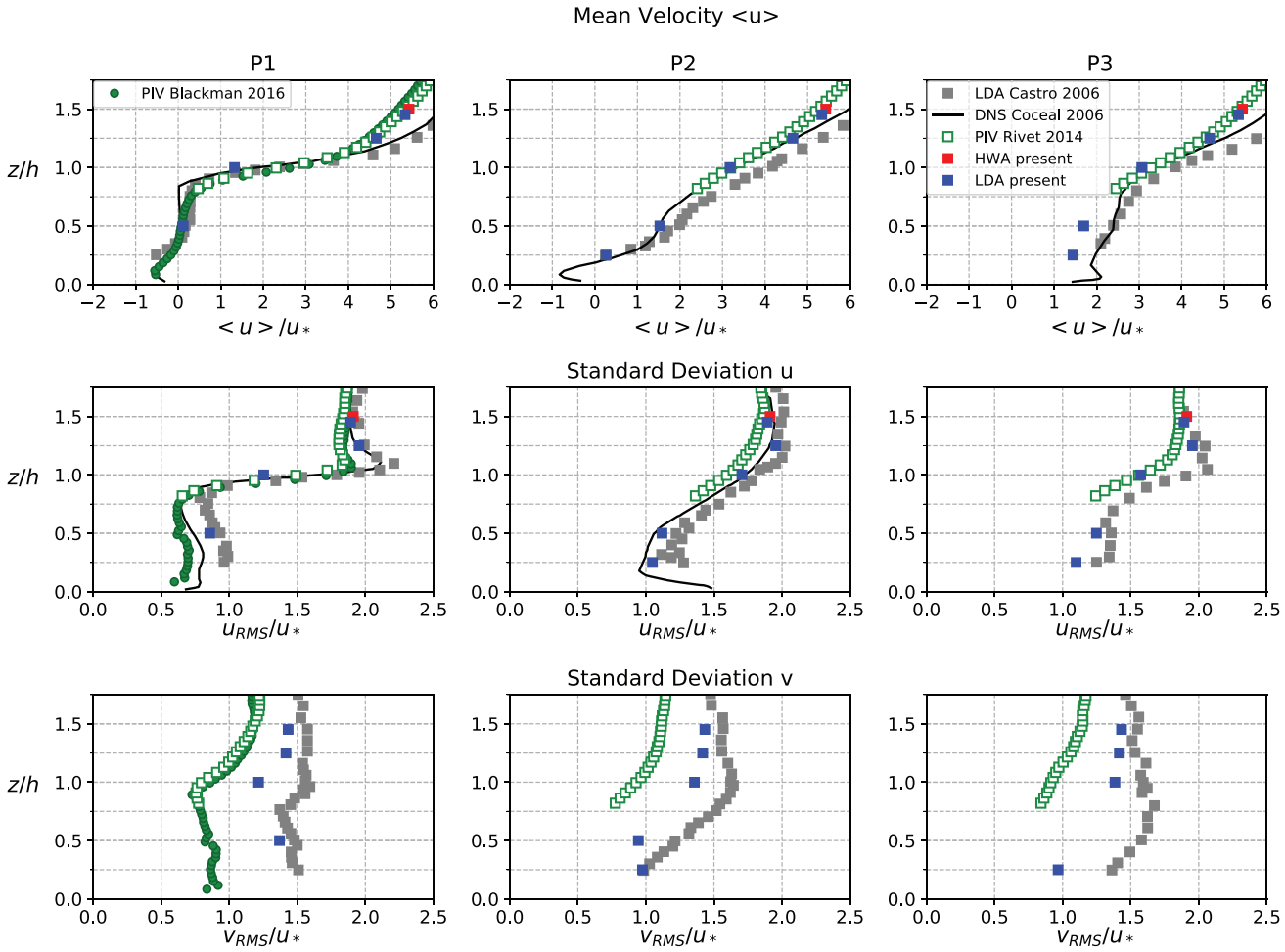

Fig. 9 Wall-normal profiles of the mean (top row) and standard deviation of the streamwise velocity component (middle row), and standard deviation of spanwise velocity component (bottom row), at P1 (left column), P2 (middle column), P3 (right column); Present LDA data are in blue symbols, compared with LDA data from Castro et al. (2006) in grey symbols, DNS data from Coceal et al. (2007) in black line, along with PIV data from Rivet (2014) (green open symbols) and Blackman and Perret (2016) (green filled symbols). The velocity at $z = 1.5h$ measured in the present study with HWA is indicated with a red symbol

3.3 Spatial distribution of power spectra density (PSD) inside the canopy

The PSD of LDA data were computed using the refined Sampled and Hold algorithm with $R(0)$ noise correction. For each measurement point, the re-sampling of the Sample and Hold interpolation scheme was performed at a frequency equal to two times the mean data rate. A block size of $T_c = 0.8\text{s} = 6.6t_{\text{inner}} = 4t_{\text{outer}}$ was used for spectra computation in the canopy (where $t_{\text{inner}} = h/u_*$ and $t_{\text{outer}} = \delta/U_e$).

3.3.1 PSD of the streamwise velocity

The overall influence of wall-normal distance on the spectral distribution of energy is first analyzed using the pre-multiplied PSD of the streamwise velocity component obtained from LDA data at the different heights inside the canopy: $z = h/4$, $z = h/2$, $z = h$ (Fig. 10). At given height, the spectra are averaged between all measurement points, the influence of the measurement station inside the canopy will be detailed in the next paragraph. To extend this analysis to the roughness sublayer and inertial layer, we included the PSD measured above the canopy interface at point E, in the roughness sub-layer at $z = 1.25h$, $z = 1.45h$, and $z = 5h$ (grey and black lines).

The power spectra is found to have the highest level (more energy) in the roughness sub-layer at $z = 1.25h$ and $z = 1.45h$, followed by the inertial region ($z = 5h$), and finally by the canopy (less energy). Inside the canopy, the energy is the highest at the canopy interface ($z = h$) and then decreases with decreasing wall-normal distance, down to $z = h/2$. In the vicinity of the wall ($z = h/2$ and h / 4), the level of energy is low and stable (little variation with z). In the roughness sub-layer, the peak of energy is centered at $f = U_e/\delta$, which is an indication that the flow dynamics is governed by the outer flow in this region.

The spatial evolution of the power spectra of the streamwise velocity component within wall-parallel planes inside the canopy is analyzed using Fig. 11 at $z = h$ (top), $z = h/2$ (middle), and $z = h/4$ (bottom) with a linear-log representation (left) and a log-log representation (right). On the logarithmic representation, a black line with $-2/3$ slope is shown (equivalent to the $-5/3$ in the non-premultiplied form), to allow for comparison with the logarithmic region classically found in the inertial range of turbulent flows.

At the canopy interface ($z = h$), the energy is found to be spatially homogeneous as observed on the u_{RMS} distribution in Fig. 7, except in the downstream region of a cube (P1 and D), where the energy level is lower and shifted towards higher frequencies, which is probably the signature of the shear layer from the trailing edge of the cube. All spectra show a good collapse in the inertial subrange and display a logarithmic region with a slope close to $-2/3$. At mid-height of the canopy ($z = h/2$), there is more energy in a streamwise alley in between two cubes (C, P3, B), with the highest level at point C. An intermediate level is obtained in the upstream region (A, P2) and a low level is found again in the downstream region (P1) of a cube due to the low dynamic of the flow in the recirculation region. The spectra only tangentially approach the $-2/3$ region, and due to the variance of the spectra in the high-frequency region, a clear inertial region at the canopy mid-height cannot be evidenced. In any case, this region would be of fairly limited extent. Close to the wall ($z/h = 1/4$), we only have data at points P2, P3, and B. The maximum of energy is obtained at point B probably induced by high fluctuations due to the separation occurring on the side of the cube, as also observed at $z/h = 1/2$ for point C (in close vicinity of B).

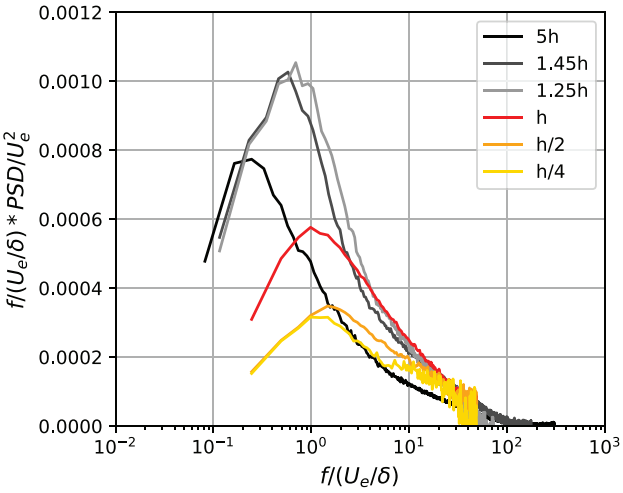

Fig. 10 Wall-normal evolution of the pre-multiplied power spectral density of the streamwise velocity component from LDA data, in outer scaling. The spectra above the canopy ($z = 5, 1.45, 1.25h$) are taken at point E; the spectra inside the canopy ($z = h, h/2, h/4$) are averaged between all measurement points

In Fig. 12 we report the frequency of the main energetic peak extracted for each measured point, while in Fig. 13, we report the average position of this peak in each wall-parallel planes. The peak frequency above the canopy at point E is showed in order to get a more complete view on the evolution of peak frequency as a function of wall-normal distance. Overall, the average frequency of the main peak of energy is a decreasing function of wall-normal distance. At point E in the inertial layer, the peak frequency is the lowest and reads $f_{\mathrm{peak}} = 0.25U_e/\delta$; using a Taylor hypothesis, this yields a characteristic size of the large-scale motions of 3δ in the inertial layer. When going down towards the wall, the peak frequency increases, with a change of slope at point E in the roughness sub-layer ($z/h = 1.5$), which can be interpreted as a footprint of the cube on the dynamics of the flow. The peak frequency is homogeneous at the canopy at the canopy interface ($z = h$), with a peak frequency being located precisely at the characteristic frequency of outer-scaled motions $f_{\mathrm{peak}} = f_{\mathrm{outer}} = U_e/\delta$ except for the downstream region of the cube (P1 and D) who have a peak frequency being more than twice as high as the other points due to their position within the shear layer developing from the top edge of the cube. Deeper inside the canopy ($z = h/2$, h / 4), there is more spatial heterogeneity, but overall the average peak frequency shows a linear evolution in the region $z/h \in [0.5 : 1.45]$.

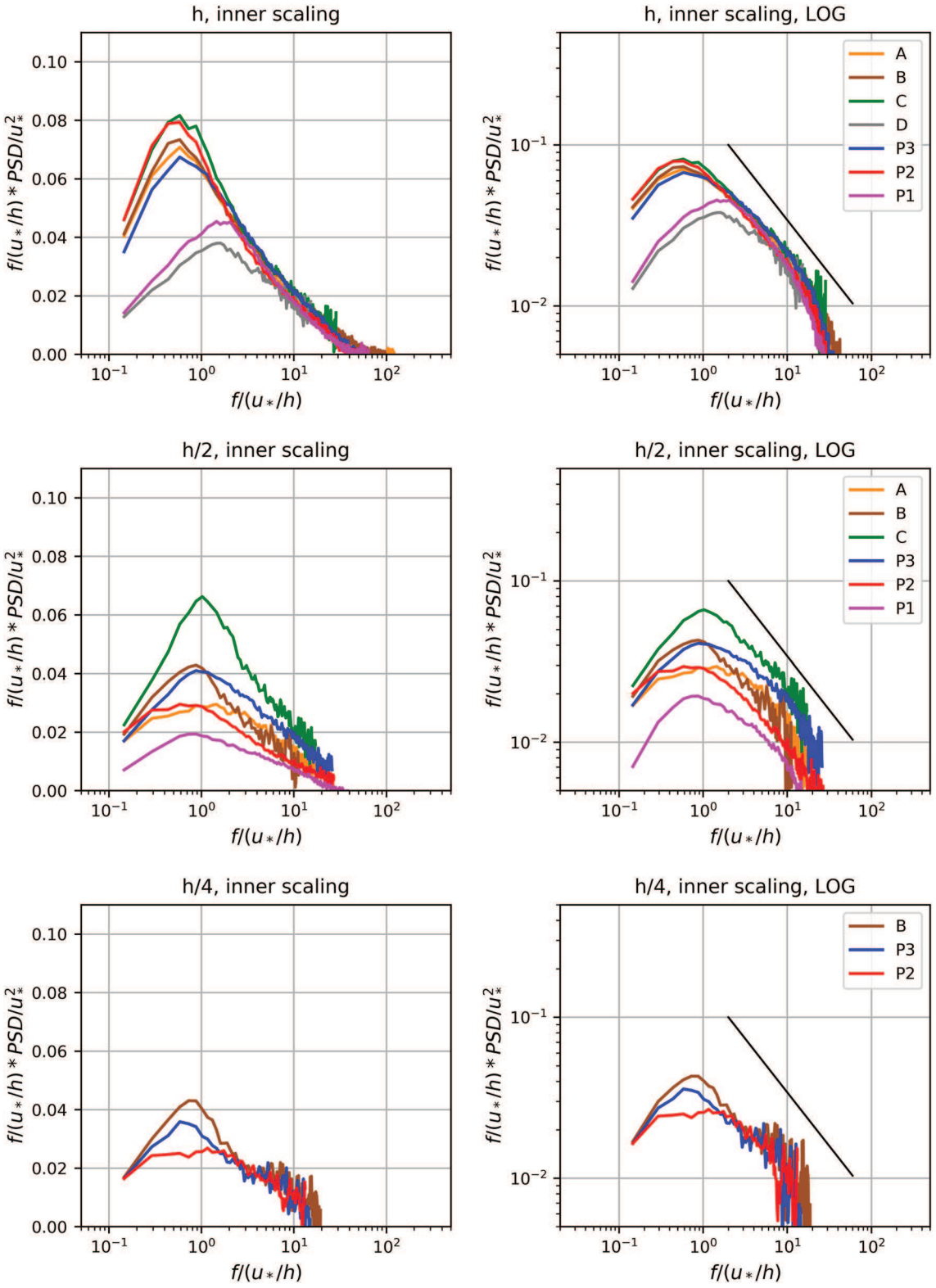

Fig. 11 Pre-multiplied power spectral density of the streamwise velocity component from LDA data, at all measurement points and at all heights, in linear-logarithmic scale (left column) and in logarithmic-logarithmic scale (right column)

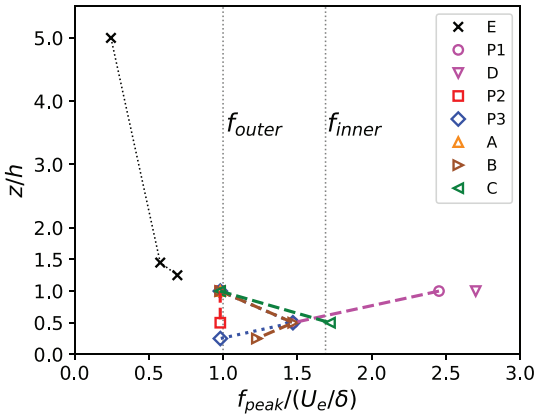

Fig. 12 Evolution of the peak of maximum energy of the pre-multiplied power spectral density of the streamwise velocity component

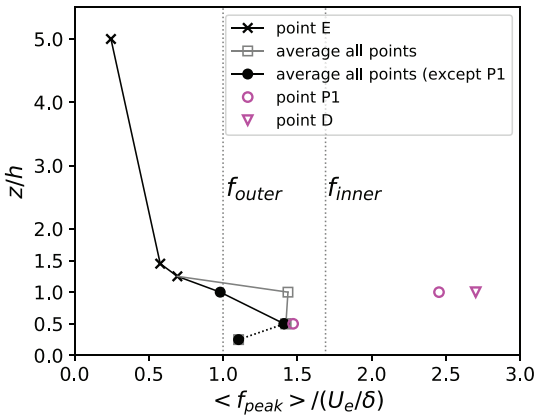

Fig. 13 Average position of the peak of maximum energy of the pre-multiplied power spectral density of the streamwise velocity component

Overall, the peak frequency is the highest at the canopy mid-height, with the highest frequency obtained at points P3, C and B with $f_{\text{peak}} \approx f_{\text{inner}} = u_*/h$, and then decreases towards a lower frequency at $z/h = 1/4$. However, in the upstream region of a cube (P2), the peak frequency remains constant through out the canopy, at the lowest frequency $f_{\text{peak}} = f_{\text{outer}}$. It should be noted that at $z/h = 1/4$, the average is less representative of the full canopy pattern because only three points (P2, P3 and B) were measured, and a reliable peak frequency at P2 could not be extracted due to the "plateau" shape of the PSD at that point. If the assumption is made that the shift towards higher frequencies is linked to the influence of the cube on the flow dynamics, then the downstream region of the cube (P1 and D) are the most impacted by the cube dynamics and the least impacted by the outer flow; on the contrary, the upstream region of the cube (P2) is the most impacted by the outer flow. In addition, it is likely that points having a peak frequency located between f_{inner} and f_{outer} feel both dynamics of inner- and outer-flow, in connection with the complex scale-interactions in these regions.

3.3.2 PSD of the spanwise velocity

It was checked over a wide range of frequencies that the non-premultiplied PSD (not shown here) of the spanwise component v does not contain any peak that would be characteristic of a periodic vortex shedding on the sides of the cubes. This absence of footprint of a periodic vortex shedding in our data can have two explanations: either the vortex shedding is not periodic for a canopy in the wake interference regime due to the multiple cube-to-cube interactions—this hypothesis is supported by the work of Castro and Robins (1977) who also argue that large δ/h ratio may affect the vortex shedding due to increased upstream turbulence ; alternatively, the fact that we do not observe vortex-shedding could be related to a limitation of pointwise measurements, especially in case of intermittent flapping of the shear layer on the sides of the cube.

The average wall-normal evolution of the pre-multiplied power spectra for the spanwise velocity component is shown in Fig. 14 in outer scaling. Overall the influence of the wall-normal distance is less noticeable on the PSD of v than on the PSD of u. Above the canopy, in the inertial region and the roughness sublayer, the PSD of v is divided by a factor 2 compared to the one obtained previously for u. In contrast, inside the canopy, u and v have similar energy levels, probably because the flow is highly three-dimensional in this region.

The distribution of pre-multiplied PSD of the spanwise velocity component within wall-parallel planes, at each measured point in the canopy is shown in Fig. 15 in linear-log (left column) and log-log (right column) representations. Interestingly, the PSD of v is found to be very energetic at point B throughout the canopy. At the canopy interface ($z = h$), all points show a peak of energy that is lower and broader than on the u component, meaning that the energy is lower and distributed over a wider range of frequencies. The spectra do not display a clear logarithmic region. At point P1 the broadening of the peak is such that it is followed by a plateau spanning half a decade of frequency. At the canopy mid-height, the main peak at low frequency ($f = U_e/\delta$) is very energetic for point B and point P1, indicating a strong influence of the outer flow at these locations inside the canopy, or a redistribution of energy between the u and v components. On the high wavenumber side, the higher level of energy observed at the corner of the cube and in the streamwise alley (B and C) can be associated to the wake or to the flapping of the flow next to the cube. Closer to the wall ($z = h/4$), the energy level at high frequencies is the same as for $z = h/2$ for points B and P2. In particular, the secondary peak is still visible in point B. The point in the streamwise

alley of a cube P3 show a good collapse with point B in the high frequency range.

In Fig. 16 we report the frequency of the peak of energy extracted for each point. For the canopy interface at $z = h$, the peak has been extracted for all points. At $z = h/2$ and $z = h/4$, the peak was extracted only where a clear peak was visible on the pre-multiplied plots; when the spectra display a plateau behavior, extracting a peak frequency did not seem relevant. Therefore, the main peak of the PSD of v has only been extracted for P1 and B for $z = h/2$ and $z = h/4$. The range of frequencies involved in the peak of energy is broader on v ($f_{\text{peak}}\delta/U_e \in [0.4 : 2]$) than on u ($f_{\text{peak}}\delta/U_e \in [0.6 : 1.4]$). Above the canopy (point E), the peak frequency of the v component is a decreasing function of wall distance, and is located at higher frequency than the u component, indicating that the spanwise velocity component is more affected by the cube dynamics than the streamwise component. At the canopy interface, the peak frequency is no longer identical for all points, and there is more spatial variation within wall-parallel planes at all heights within the canopy. This variation can be explained by the broadening of the PSD of v and the plateau/two-peaks behavior observed at certain points. For point B, which has the highest level of energy, the frequency is the lowest and decreases with decreasing wall-normal distance. The peak frequency at the canopy interface is found to be is the highest at point P3.

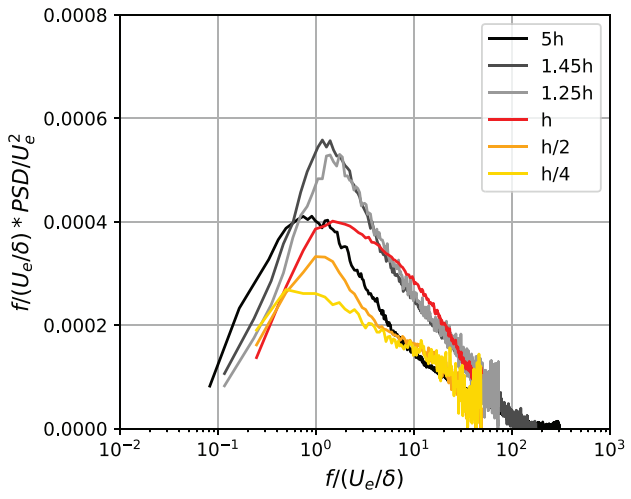

Fig. 14 Wall-normal evolution of the pre-multiplied power spectral density of the spanwise velocity component from LDA data, in outer scaling. The spectra above the canopy ($z = 5, 1.45, 1.25h$) are taken at point E; the spectra inside the canopy ($z = h, h/2, h/4$) are averaged between all measurement points

3.4 Integral time scale of the flow

The integral time scale of the flow represents the duration over which the velocity component u_i is correlated with itself. It is defined as the extent of an equivalent (in the integral sense) correlation with a rectangular shape and a height of 1 (see Eq. 2).

$$\Lambda_{u_i,t} = \int_0^\infty R_{u_i u_i}(\Delta t) d(\Delta t) \tag{2}$$

where $R_{u_i u_i}$ is the correlation coefficient of velocity component u_i, i.e., the auto-correlation normalized by the value at zero time lag $R_{u_i u_i}(\Delta t = 0)$. The temporal auto-correlation is computed from the LDA data using the Refined Sample and Hold algorithm (Nobach et al. 1998) already described in Sect. 2.2. The integral time-scale is computed by integrating the auto-correlation from zero time lag to the first zero-correlation crossing. The auto-correlation coefficient of the streamwise component at $z = h/2$ is shown in Fig. 17 for all points.

The wall-normal evolution of the integral time scale of the streamwise velocity component for each measured point inside the canopy, at the canopy interface, and above the canopy are shown in Fig. 18, non-dimensionalized using the cube height h and the friction velocity u_*. The average integral scale at each height z is plotted with a dashed line. As it can be seen, the average integral timescale remains approximately constant throughout the canopy height, with $\Lambda_{u,t} = 0.2 \times h/u_* = 0.2 \times t_{\text{inner}}$. In the roughness sublayer the integral time scale then increases with increasing wall-normal distance. Looking at the detail of each measured points, it is of interest to note that the timescale of the flow is spatially homogeneous at $z = h$, except at point P1 with a significantly lower timescale. This is consistent with the analysis of the power spectral density carried out in Sect. 3.3, where it was shown that the frequency of the peak of energy at P1 and $z = h$ was higher than at other locations in the canopy. The timescales measured at $z = h/4$ are also spatially homogeneous. Some degree of heterogeneity is found at $z = h/2$.

Even if the mean flow is not spatially homogeneous in the canopy, we found that at given height, the degree of heterogeneity of the power spectral density and the correlation coefficient is fairly limited, except in the recirculation region of a cube at point P1. Thus, even if the Taylor hypothesis is not strictly valid, it is still of interest to attempt to use it to retrieve the integral length scale out of the time scale. The convection velocity at height z is chosen as $\langle u(z) \rangle$, the average streamwise velocity in the (x, y) plane. The results are shown in Fig. 19. At given height, the collapse of all measured points appears even better than the for the integral time scale, with a better collapse of all points (P1 excepted) on the average length

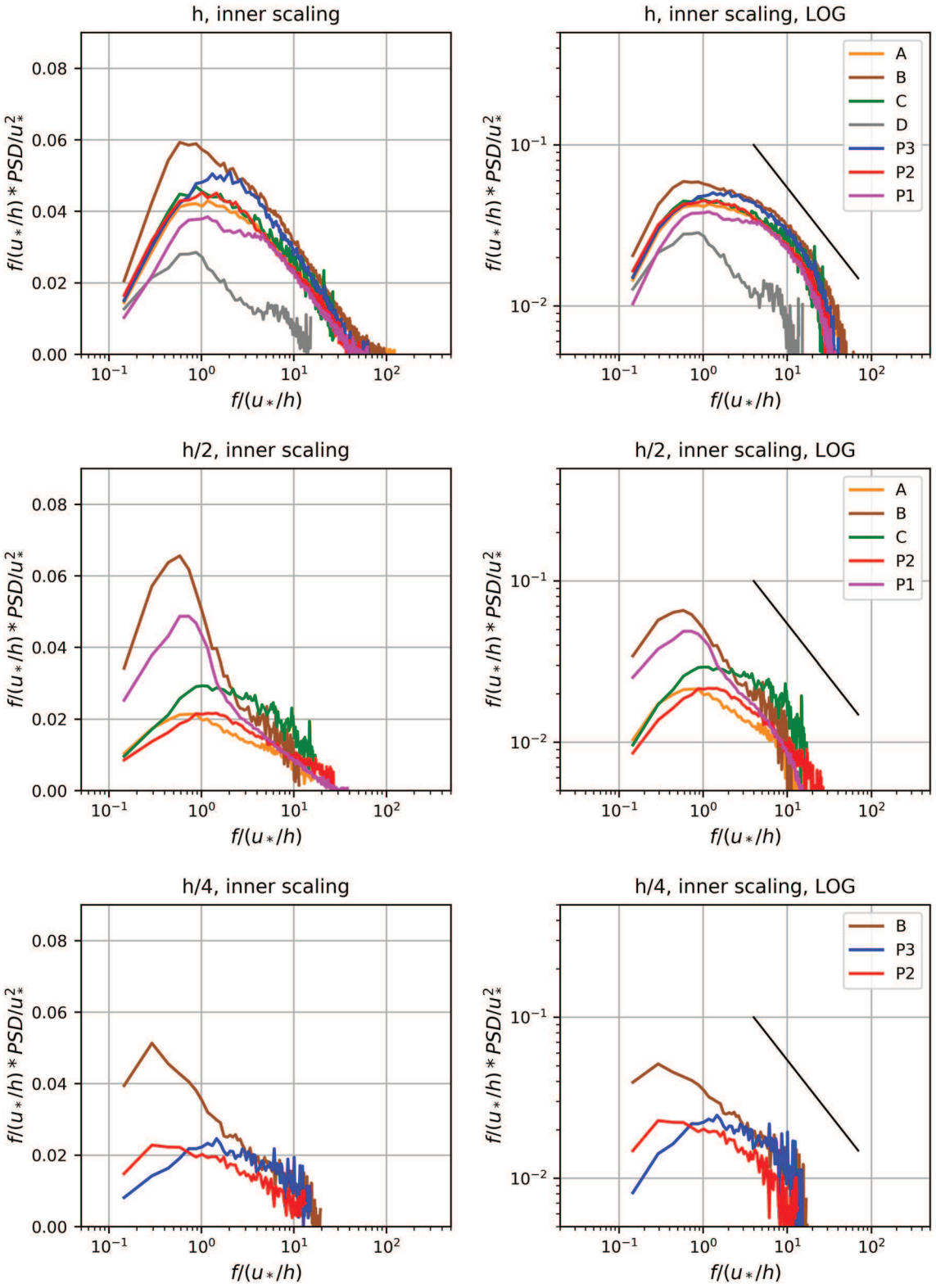

Fig. 15 Pre-multiplied power spectral density of the spanwise velocity component from LDA data, at all measurement points and at all heights

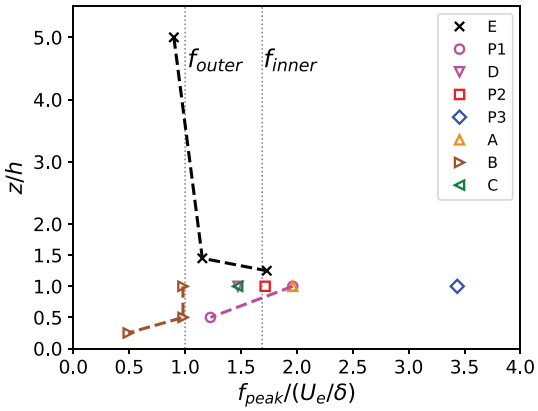

Fig. 16 Evolution of the peak of maximum energy of the pre-multiplied power spectral density of the spanwise velocity component

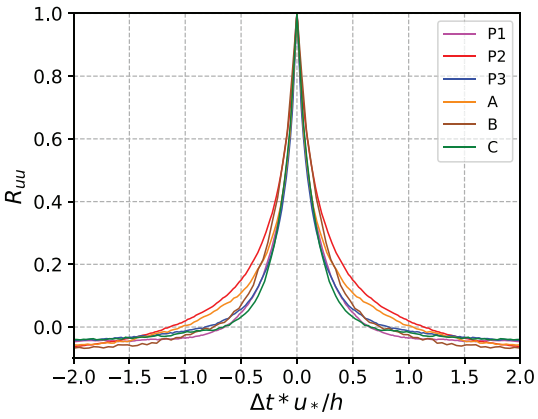

Fig. 17 Correlation coefficient of the streamwise velocity component R_{uu} at $z = h/2$

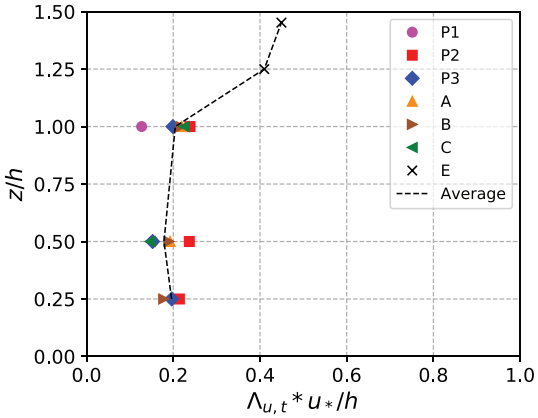

Fig. 18 Wall-normal evolution of the integral time scale of the flow

scale. This average length scale is roughly constant at $z = h/4$ and $z = h/2$, with $\Lambda_{u,x} = h/4$. The length scale then increases with increasing wall-normal distance, with a sharp increase

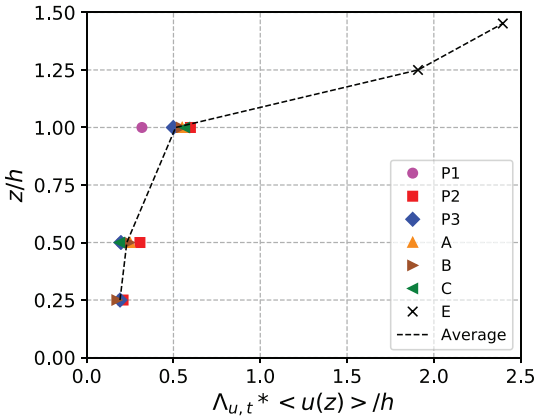

Fig. 19 Wall-normal evolution of the integral time scale of the streamwise velocity component, converted to a length scale using a Taylor hypothesis

just above the canopy interface. In comparison with $z = h/4$, the integral length scale at $z = 1.45h$ is multiplied by a factor 10 to reach a value of $\Lambda_{u,x} = 2.5h$. This value is close to $3h$, the canopy pattern streamwise separation between two cubes. Thanks to the use of the Taylor hypothesis, it is also possible to compare the present results with the data from Reynolds and Castro (2008) obtained with PIV at points P1 and P2. Because of the limited extent of the field of view, they used an alternative definition of the integral scale, given by the separation at which the correlation coefficient falls down to 0.5:

$$R_{u_i u_i}(\Lambda_{1/2}) = 0.5 \tag{3}$$

The comparison of the present results re-computed using this definition of the integral length scale $\Lambda_{1/2}$ with the results from Reynolds and Castro (2008) is shown in Fig. 20. The two datasets are in excellent agreement at point P2 throughout the canopy height and also in the roughness sublayer. This confirms that, the Taylor hypothesis seems valid at point P2 in the canopy. Because the two datasets are in different conditions in terms of Reynolds number and boundary layer thickness to cube height ratio, this good collapse of the data is also a strong indication that the inner scaling given by h and u_* is appropriate for the canopy.

Finally, the correlation coefficient and the integral time scale of the spanwise velocity component is shown in Figs. 21 and 22, respectively. While the time-scale of the spanwise velocity component appears fully homogeneous at the canopy interface $z = h$ (including P1), there is more spatial heterogeneity at $z = h/2$ and $z = h/4$ than on the streamwise velocity component. In particular, the temporal time-scale is found to increase with decreasing wall-normal distance for points B and P1, which exhibits the largest time-scale at the canopy mid-height. This is in good agreement with the Power Spectral Density analysis where a stronger energy peak was obtained at low frequency in the

downstream region and at the corner of the cube (Fig. 15), and also with the maps of standard deviation of the spanwise velocity (Fig. 7). This can be attributed to the slow oscillations of the flow in the horizontal plane, with the flow being "channeled" along the diagonal alleys that exist in a staggered cube array.

3.5 Coherence between the canopy flow and the boundary layer flow

The linear interaction between the different flow regions is investigated through the analysis of the coherence between the streamwise velocity measured inside the canopy using LDA with the streamwise velocity measured at $z = 1.5h$ and $z = 5h$ using HWA. The coherence is defined as:

$$\gamma^2 = \frac{|\langle U_{canopy}(f)\overline{U_{outer\ flow}(f)}\rangle|^2}{\langle|U_{canopy}(f)|^2\rangle\langle|U_{outer\ flow}(f)|^2\rangle} \tag{4}$$

where $\langle\rangle$ denotes ensemble averaging, the overbar indicate the complex conjugate, $||$ is the modulus. The coherence between two signals is the spectral equivalent of the cross-correlation in the temporal domain. It is normalized by the PSD of each signal, such that it takes values ranging from 0 (no coherence) to 1 (full coherence).

We first examine the coherence between the roughness sublayer at $z = 1.5h$ and the inertial layer at $z = 5h$ using the coherence between the two hot-wire signals (see Fig. 23). The coherence is a decreasing function of the frequency, meaning that the long-time motions are better correlated than the short-time motions. Here, the two signals appear to have some degree of coherence for $f/(U_e/\delta) \leq 1$, or conversely for $\lambda_x \geq \delta$ using a frozen turbulence hypothesis with the mean velocity at $z = 5h$ taken as the local convection velocity. The coherence between the two flow regions reaches a maximum level of $\gamma^2 = 0.45$ for long-time motions, at $f/(U_e/\delta) \approx 10^{-2}$, or conversely for large-scale motions with $\lambda_x = 40\delta$. As suggested by Baars et al. (2016), a cut-off frequency can be defined for short-time motions using a coherence threshold level $\gamma_{\min} = 0.05$, for which linear interactions become negligible. For our urban boundary layer flow, it is of the order of $f_{cut,\gamma} \approx 0.4U_e/\delta$, or conversely in wavenumber $\lambda_{cut,\gamma} \approx 1.8\delta$. It is of interest to compare these values to those obtained for a turbulent boundary layer over a flat plate : Baars et al. (2016) obtained a maximum coherence of $\gamma^2 = 0.8$ at equivalent wavelength ($\lambda_x = 40\delta$), and a threshold $\lambda_{cut,\gamma} \approx 0.45\delta$ between two points located at $z^+ = 10.5$ (in the buffer region) and $z^+ = 469$ (beginning of the logarithmic region), inside a turbulent boundary layer flow at $\delta^+ = 13300$. Although it is difficult to compare the results in the context of two flows of different nature, the results obtained for the urban boundary layer

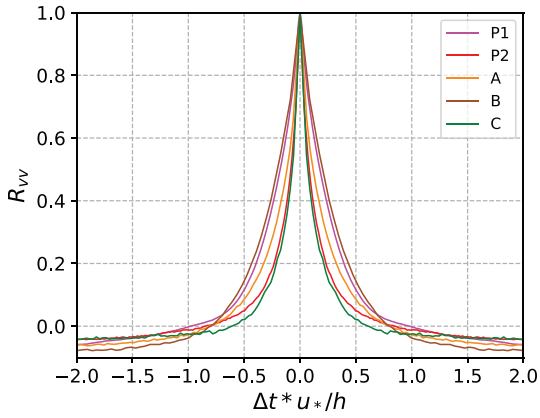

Fig. 21 Correlation coefficient of the spanwise velocity component R_{vv} at $z = h/2$

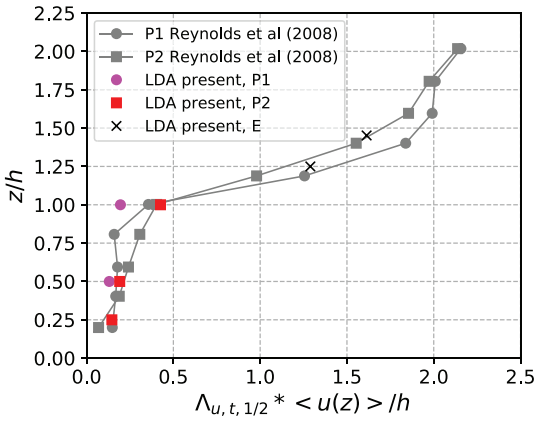

Fig. 20 Integral scale of the streamwise velocity component, compared to Reynolds and Castro (2008) using a Taylor hypothesis

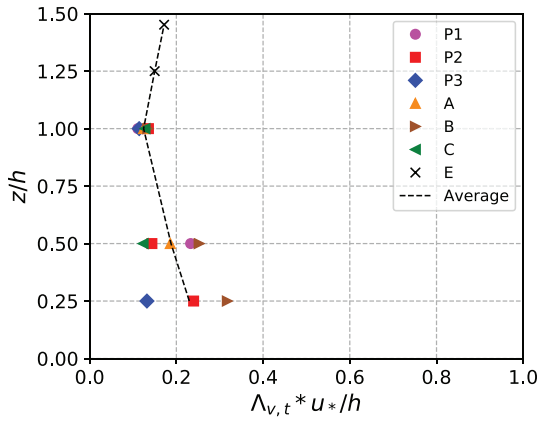

Fig. 22 Wall-normal evolution of the integral time scale of the spanwise velocity component

flow seem to indicate that the linear interactions between the inner-wall region and the inertial region is weaker than in the smooth-wall flow, with a lower coherence level and a higher cut-off wavelength.

The coherence between the streamwise velocity inside the canopy and in the outer flow is now analyzed using the LDA measurements in the canopy and the HWA measurements in the roughness sublayer ($z = 1.5h$) and in the inertial sublayer ($z = 5h$) (Fig. 24). Overall, the coherence of the canopy is stronger with the roughness sublayer than with the inertial layer, and the degree of coherence decreases with decreasing wall-normal distance inside the canopy. This is consistent with the variation of the separation distance between the two measurement points: the closer the two measurement points, the higher the overall degree of coherence between the two signals.

Looking into more details into the coherence between the roughness sublayer and the canopy interface ($z = h$), there is a strong spatial heterogeneity depending on the location inside the canopy, with three groups of LDA points : the highest coherence ($\gamma^2 = 0.6$) is obtained in the vicinity of the cubes (upstream and corner region with points B, C and A). This is an indication that the turbulence in the roughness sublayer is influenced by the shear layers and wakes originating from the cubes. An intermediate coherence is obtained for P3, P2, and D, and finally a low degree of coherence in the cube downstream region (P1). At the canopy mid-height, the level of coherence is decreased; in particular, C and P1 have a coherence close to zero. Close to the wall ($z = h/4$), points P3 and B still show some degree of coherence, but the upstream region of the cube (P2) appears disconnected from the outer flow.

This is quite consistent with this measurement position being located inside the cube upstream horseshoe vortex; this is also consistent with the analysis of the wall-normal evolution of u_{RMS}.

The analysis of the coherence of the LDA points inside the canopy with the inertial layer, besides a lower level coherence, also show a more uniform behavior among all LDA points. Although the differences are less significant, points B, P3, and A still show a higher level of coherence, point P1 a lower level of coherence.

The low degree of coherence for P1 (downstream region of the cube) observed throughout the canopy height is consistent with the analysis of the power spectra in the canopy, where this point was shown to have a low energy level, shifted towards higher frequency. It confirms that, due to a sheltering effect of the cube, P1 only see the cube dynamics, and is not influenced by the outer flow dynamics.

The wall-normal evolution of the coherence cut-off frequency and wavenumber is shown in Fig. 25a, b. As both subplots give the same information, but in two different representations, only the frequency plot will be commented below. Overall, it can be seen that the coherence range is restricted to rather low frequencies, and is narrowing down with decreasing wall normal distance. The canopy exhibits a larger coherence range with the roughness sublayer than with the inertial layer, and in both cases the cut-off frequency decreases with decreasing wall-normal distance.

The cut-off frequency of the canopy with the inertial layer appears spatially homogeneous at the canopy interface, with all LDA points yielding $f_{\mathrm{cut},\gamma} \approx 0.28$ in outer scaling. This cut-off frequency is of the same order (but slightly higher) than the frequency of the peak of maximum energy at $z = 5h$: $f_{\mathrm{peak},5h} \approx 0.23$, meaning that the coherence range does

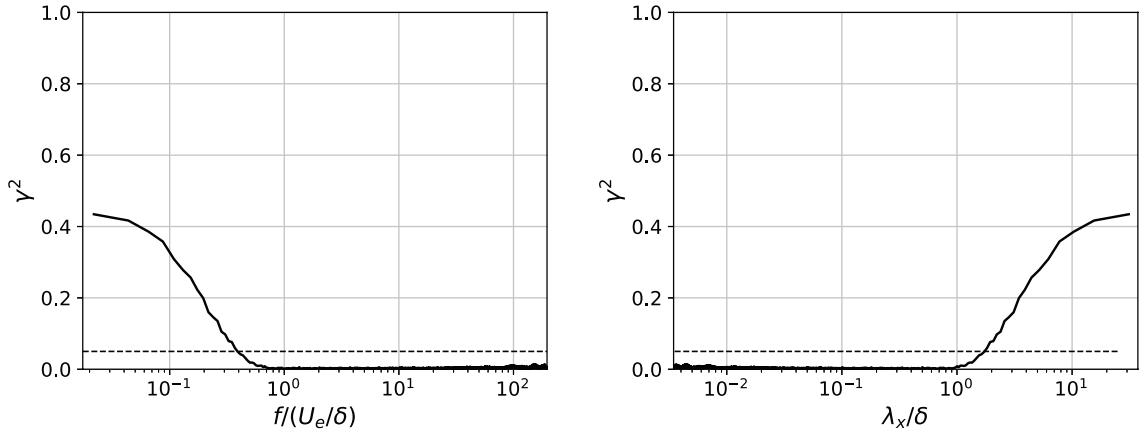

(a) frequency representation **(b)** wavelength representation

Fig. 23 Coherence of the streamwise velocity between the roughness sublayer at $z = 1.5h$ and the inertial layer at $z = 5h$, computed with the HWA signal; the dashed line indicates a coherence threshold level of $\gamma^2 = 0.05$, used for computation of the cut-off frequency or wavelength

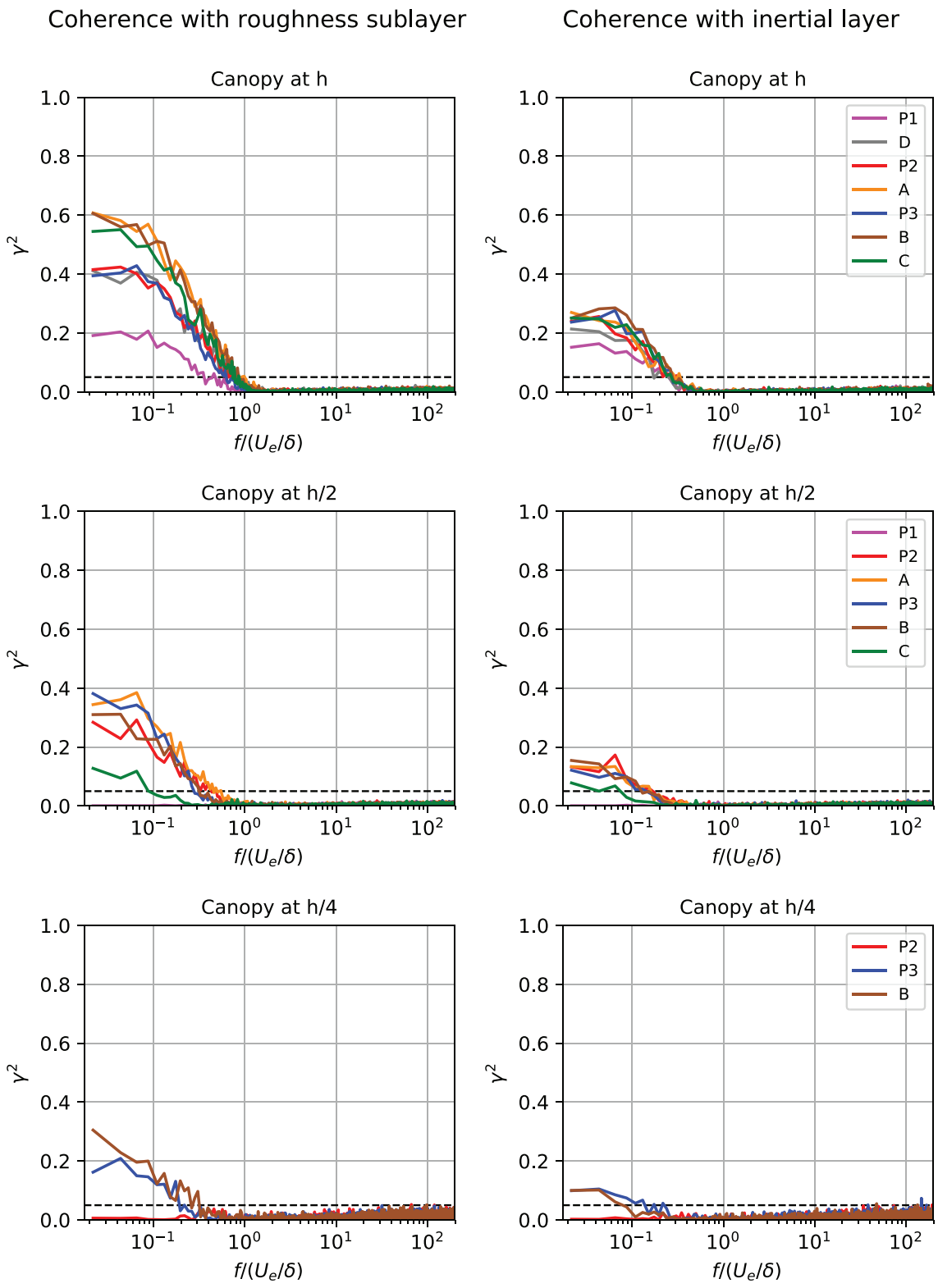

Fig. 24 Coherence of the HWA streamwise velocity in the roughness sublayer at $z = 1.5h$ (left) and in the inertial layer at $z = 5h$ (right) with the LDA streamwise velocity in the canopy, at $z = h$ (top), $z = h/2$ (middle), $z = h/4$ (bottom), in outer scaling. The dashed line indicates a coherence threshold level of $\gamma^2 = 0.05$, used for computation of the cut-off frequency or wavelength

have some overlap with the energy peak frequency range in the inertial layer. However, it does not include the energy peak at the canopy interface, located at higher frequency ($f_{\text{peak},h} = 1$). Deeper inside the canopy, the cut-off frequency reaches down to $f_{\text{cut},\gamma} \approx 0.07$ at $z = h/4$ for point B, and at $z = h/2$ for point C. With such a low cut-off frequency, the coherence frequency range does not overlap anymore the peak energy range in the inertial layer or in the canopy.

Looking now at the cut-off frequency of the canopy with the roughness sublayer, there is more spatial variation between the LDA points, with a cut-off frequency in the range $f_{\text{cut},\gamma} \in [0.45;0.85]$. The main peak of energy in the

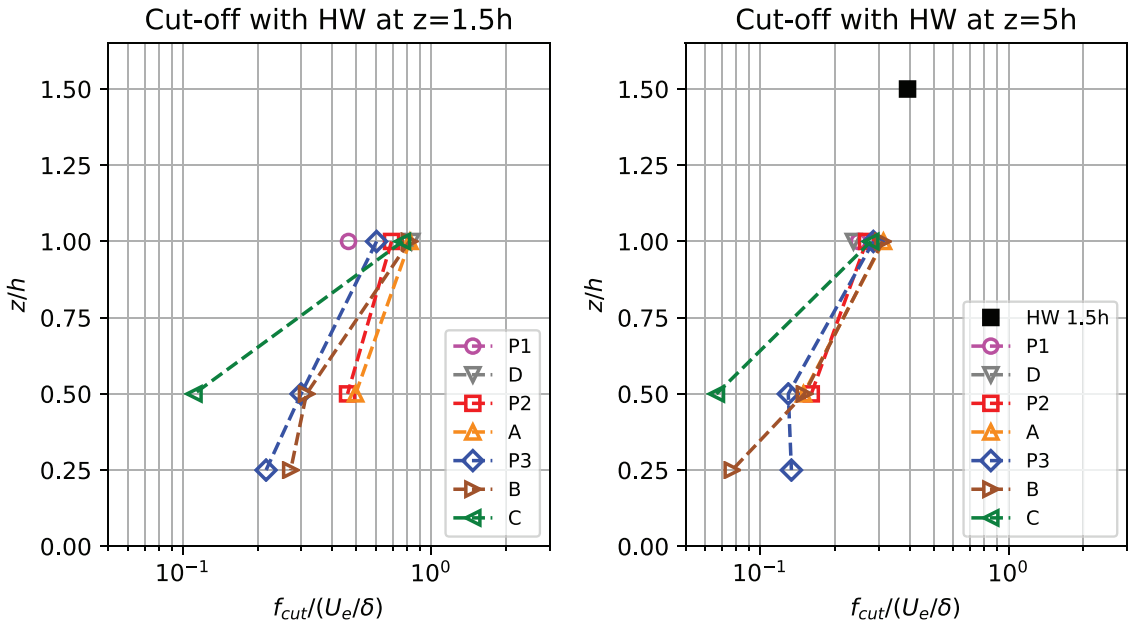

(a) Cut-off frequency

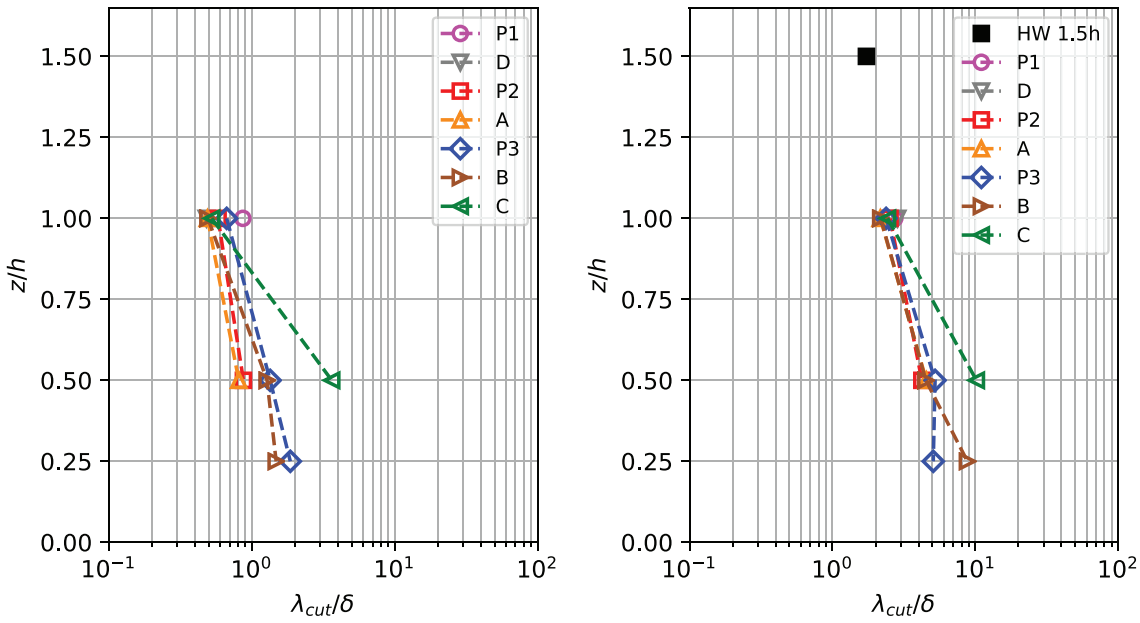

(b) Cut-off wavelength

Fig. 25 Cut-off frequency and wavelength of the coherence between the streamwise velocity in the roughness sublayer at $z = 1.5h$ (left) and in the inertial layer at $z = 5h$ (right) with the streamwise velocity in the canopy, in outer scaling

roughness sublayer is located at $f_{\text{peak},1.5h} \approx 0.55$, there is thus a significant overlap with the frequency ranges of the coherence. The extent of the coherence range is larger for all points in the vicinity of a cube: B, C, A, and D. This indicates that the dynamics of the roughness sublayer is strongly influenced by the dynamics of the flow induced by the cubes in the canopy.

3.5.1 Coherence of the spanwise velocity in the Canopy with the outer flow

The level of coherence of the spanwise velocity in the canopy is much lower than that of the streamwise velocity. Most of the LDA points do not even reach the threshold level $\Gamma_{\min} = 0.05$, so are, therefore, not worth showing in a dedicated figure. The most significant level of coherence is obtained with the roughness sublayer at point B at $z = h/2$ ($\gamma^2 \approx 0.25$) and $z = h/4$ ($\gamma^2 \approx 0.17$), possibly owing to the contribution of the wakes and shear layers on the sides of the cubes to the energy in the roughness sublayer.

4 Conclusion

The flow inside an idealized urban canopy consisting of a staggered array of cubes with a 25% density, immersed into an atmospheric boundary layer with a Reynolds number of $\delta^+ = 32{,}300$ has been investigated by means of Laser Doppler Anemometry. The cube boundary layer thickness to cube height ratio ($\delta/h = 22.7$) is large enough to be representative of atmospheric surface layer flow in neutral conditions. Measurements are realized at three heights in the canopy ($z = h/4$, $h/2$, h) and at different positions in wall-parallel planes: P1, P2, P3 are placed on symmetry axis of the canopy pattern, and allow us to perform comparison with the literature (Castro et al. 2006); additional points, called A, B, C, D are also probed with LDA to extract more information on the dynamics of the flow in the cube vicinity. The novelty part of this paper is the spatio-temporal analysis of the dynamics of the flow inside the canopy, through temporal power spectra density and auto-correlation of streamwise and spanwise velocity components at different spatial positions inside the canopy.

Analysis of wall-parallel maps and wall-normal profiles of mean and standard deviation of both velocity components has shown an overall good agreement with available data in the literature, which confirms that the inner-scaling (with u_* and h) is appropriate for the canopy region. It should, however, be noted that some differences are observed on the standard deviation of the spanwise velocity component, particularly between PIV and LDA measurement techniques. Overall, the flow appears well homogeneous at the top of the canopy, and becomes more heterogeneous as approaching the wall, which is supported by the PSD of u- and v-components in wall-parallel planes within the canopy.

The wall-normal evolution of the PSD of the streamwise velocity component u shows the following noticeable facts:

- in the inertial layer, the size of the large-scale motions given by the frequency of the main peak of energy is of the order of 3δ, as classically observed in turbulent wall-bounded flows;
- the influence of the wall roughness extends above the canopy, and is visible through a shift of energy towards higher frequencies with decreasing wall-normal distance; in particular, the roughness sublayer is the region that exhibits the sharpest increase in frequency of the main peak of energy;
- at the canopy interface and above a logarithmic region of slope close to $-5/3$ is evidenced; this is not the case deeper inside the canopy.
- within the canopy, the main peak of energy is located at $f = U_e/\delta$, indicating that energy is extracted from the outer flow; the influence of the wall roughness is also felt through a broadening of the energy peak towards higher frequency;
- the integral time-scale of the flow remains homogeneous through the canopy depth, with $\Lambda_{u,t} = 0.2 \times h/u_*$;
- a specific behavior of the flow is evidenced in the downstream region of the cube. A stronger dissipation is visible through a lower level of energy and a characteristic frequency two-times higher than other points at the canopy interface. This indicates a stronger influence of the cube in this flow region.

An attempt to compare integral time scales obtained here with integral length scale results produced by Reynolds and Castro (2008) is made using Taylor's hypothesis. The agreement is excellent in the upstream region of the cube, but differences are observed in the sheltered region behind the cube. In both datasets, the integral length scale is about $h/3$ at the canopy mid-height and undergoes a sharp increase through the canopy interface to reach a value close to $3h$ in the roughness sublayer (matching the inter-cube streamwise separation).

In the PSD of the spanwise velocity component v, the main peak of energy is located at $f_{\text{peak}} = U_e/\delta$ (similarly as the PSD of u), indicating that the turbulent energy is also extracted from the outer flow. A higher level of energy is however obtained at the corner of cubes at mid-height of the canopy due to the flow separation and shear layer originated from the sharp edges on the sides of the cube. In contrast with the findings of Meinders and Hanjalic (1999), no footprint of a periodic vortex shedding on the sides of the cubes could be clearly evidenced. The absence of clear periodic vortex shedding can be explained by the multiple cube

interactions in the wake interference regime and to the large δ/h ratio (Castro and Robins 1977). However, an interesting phenomenon is observed on the PSD of v with a broadening of the energy peak towards higher frequencies which suggests the emergence of a secondary peak at $f_{peak} = 4 \times f_{inner}$, consistent with the integral time scale obtained near the corner of the cube at $z = h/2$. This behavior is consistent with the findings of Inagaki and Kanda (2008) in in-situ experiments.

The complex spatio-temporal organisation of the flow described above leads to question what does this implies in term of scale interaction between the different regions above and inside the canopy. Indeed, the energy in the low frequency domain can be attributed to the influence of the large-scale motions in the outer flow, while the energy in the high frequency domain is linked to the wake activity of the cubes. Coherence results on the streamwise velocity component obtained between the different flow regions allow to quantify the linear interactions mechanisms at stake. The salient features are summarized below:

- linear interactions between the inertial layer and the roughness sublayer are evidenced in the low-frequency range with $\gamma^2_{max} = 0.45$; this coherence level, although significant, is lower than for smooth wall boundary layer flow (Baars et al. 2016) where a maximum coherence level of $\gamma^2 = 0.8$ was observed between the viscous wall region and the logarithmic layer. However, it is worth noting that this maximum is reached at equivalent wavelength for both flows ($\lambda_x = 40\delta$);
- linear interactions are also evidenced between the canopy region and the roughness sublayer with $\gamma^2_{max} \in [0.2;0.6]$, depending on the depth inside the canopy; at given height, strong spatial heterogeneity is observed; the points in the upstream and side neighbourhood of the cubes have the highest level of coherence, indicating the contribution of the shear layers and wakes induced by the cubes to the turbulence in the roughness sublayer; in contrast, the lowest level of coherence is consistently observed in the downstream region of the cubes, which confirms the sheltering effect of the cubes;
- a rather low level of coherence is obtained between the canopy and the inertial layer with $\gamma^2 \leq 0.3$ for all points. At the canopy interface, the cut-off wavelength is homogeneous and reads $\lambda_{x,cut} = 2.5\delta$
- the extent of the coherence range in the urban roughness boundary layer flow is reduced compared to smooth-wall flow, and is narrowing down when going deeper inside the canopy. In particular, the coherence range at the canopy interface show some overlap with the main peak of energy in the roughness sublayer, and to a lesser extent with that of the inertial layer.

This body of results tends to indicate that the linear interactions in the urban roughness flow are reduced compared to smooth-wall flow. This trend is supported by the results of Squire et al. (2016) who compared the interaction mechanisms in a smooth wall turbulent boundary layer and in a sand-rough boundary layer, in the framework of the MMH model (Marusic et al. 2010). It was found that the presence of a sand-rough wall reduces the linear interactions mechanisms (superposition mechanism) and enhanced the non-linear interactions (via an amplitude modulation mechanism).

Finally, these conclusions were derived for an idealized urban canopy consisting of a staggered array of cubes with a 25% packing density, which is often chosen as a benchmark configuration in the literature. Unlike plant canopies, the wide range of geometrical parameters of the urban roughness (building shape and density, height distribution, ...), as well as the strong spatial heterogeneity of the flow inside the canopy make difficult to generalize the results obtained for one specific configuration to a wider range of geometries. However, an attempt is made below to discuss the validity of the present results for a wider range of urban canopies, in order to give more perspective to the present conclusions. Regarding the building shape, cubes are bluff and sharp edges bodies. Their specificity is that the detachment point is fixed on the edge of the body, making the aerodynamics of the flow Reynolds-number independent. The present results obtained at $h^+ = 1420$ can therefore be extended to higher Reynolds numbers. This would not be the case for rounded-edge buildings. The influence of the building densities on the flow statistics has been reviewed in Grimmond and Oke (1999), with three distinct regimes depending on the packing area density. The present canopy pertains to the wake interference regime, and it is likely that canopies with densities in the same regime (meaning between 15 and 35% density) would behave similarly, especially in terms of suppression of periodic vortex shedding, or in terms of interactions with the outer flow. In contrast, higher building densities in the skimming regime result in reduced interactions between the two flow regions, with probably lower coherence level. Finally, at given canopy densities, the influence of the cube arrangement (e.g., staggered vs aligned) and of constant height vs non-uniform height was investigated by Cheng and Castro (2002) and Coceal and Belcher (2005). The aligned cube array was found to produce the lowest drag (and hence the lower friction velocity u^*), followed by the staggered array; the non-uniform canopy showed the highest drag, resulting in an increase of the roughness sublayer thickness. It is, therefore, likely that a higher degree of coherence between the canopy flow and the roughness sublayer could be obtained for a non-uniform height canopy.

Acknowledgements The authors wish to thank the financial support of the French National Research Agency through the Research Grant URBANTURB ANR-14-CE22-0012-01, as well as Vincent Jaunet and Frank Kerhervé, assistant professors at prime laboratory in Poitiers, France, for useful advices on LDA spectra algorithms.

References

Baars WJ, Hutchins N, Marusic I (2016) Spectral stochastic estimation of high-Reynolds-number wall-bounded turbulence for a refined inner–outer interaction model. Phys Rev Fluids 1(5):054406. https://doi.org/10.1103/PhysRevFluids.1.054406

Benedict LH, Nobach H, Tropea C (2000) Estimation of turbulent velocity spectra from laser Doppler data. Meas Sci Technol 11(8):1089. https://doi.org/10.1088/0957-0233/11/8/301

Blackman K, Perret L (2016) Non-linear interactions in a boundary layer developing over an array of cubes using stochastic estimation. Phys Fluids 28(9):095108. https://doi.org/10.1063/1.4962938

Blackman K, Perret L, Calmet I, Rivet C (2017) Turbulent kinetic energy budget in the boundary layer developing over an urban-like rough wall using PIV. Phys Fluids 29(8):085,113. https://doi.org/10.1063/1.4997205

Castro IP, Robins A (1977) The flow around a surface-mounted cube in uniform and turbulent streams. J Fluid Mech 79:307–335

Castro IP, Cheng H, Reynolds R (2006) Turbulence over urban-type roughness: deductions from wind-tunnel measurements. Bound Layer Meteorol 118(1):109–131. https://doi.org/10.1007/s10546-005-5747-7

Cheng H, Castro IP (2002) Near wall flow over urban-like roughness. Bound Layer Meteorol 104(2):229–259

Coceal O, Belcher SE (2005) Mean winds through an inhomogeneous urban canopy. Bound Layer Meteorol 115(1):47–68. https://doi.org/10.1007/s10546-004-1591-4

Coceal O, Thomas TG, Castro IP, Belcher SE (2006) Mean flow and turbulence statistics over groups of urban-like cubical obstacles. Bound Layer Meteorol 121(3):491–519. https://doi.org/10.1007/s10546-006-9076-2

Coceal O, Dobre A, Thomas TG, Belcher SE (2007) Structure of turbulent flow over regular arrays of cubical roughness. J Fluid Mech. https://doi.org/10.1017/S002211200700794X

Finnigan J (2000) Turbulence in plant canopies. Ann Rev Fluid Mech 32:519–571

Grimmond C, Oke TR (1999) Aerodynamics properties of urban area derived from analysis of surface form. J Appl Meteorol 38:1262–1292

Inagaki A, Kanda M (2008) Turbulent flow similarity over an array of cubes in near-neutrally stratified atmospheric flow. J Fluid Mech 615:101. https://doi.org/10.1017/S0022112008003765

Jackson PS (1981) On the displacement height in the logarithmic velocity profile. J Fluid Mech 111:15–25

Kaimal J, Wyngaard J, Izumi Y, Cote O (1972) Spectral characteristics of surface-layer turbulence. Q J R Met Soc 98:563–589. https://doi.org/10.1002/qj.49709841707

Macdonald R, Carter S, Slawson P (2000) Measurements of mean velocity and turbulence statistics in simple obstacle arrays at 1:200 scale. Therm Fluid Rep 2000-1, Department of Mechanical Engineering, University of Waterloo

Martinuzzi R, Tropea C (1993) The flow around surface-mounted, prismatic obstacles placed in a fully developed channel flow (data bank contribution). J Fluids Eng 115(1):85–92

Martinuzzi RJ, Havel B (2004) Vortex shedding from two surface-mounted cubes in tandem. Int J Heat Fluid Flow 25(3):364–372. https://doi.org/10.1016/j.ijheatfluidflow.2004.02.003

Marusic I, Mathis R, Hutchins N (2010) Predictive model for wall-bounded turbulent flow. Science 329(5988):193–196. https://doi.org/10.1126/science.1188765

Mathis R, Hutchins N, Marusic I (2009) Large-scale amplitude modulation of the small-scale structures in turbulent boundary layers. J Fluid Mech 628:311. https://doi.org/10.1017/S0022112009006946

McKeon B, Comte-Bellot G, Foss J, Westerweel J, Scarano F, Tropea C, Meyers J, Lee J, Cavone A, Schodl R, others (2007) Handbook on experimental fluid mechanics: chapter 5: velocity, vorticity, and Mach number. In: Springer handbook of experimental fluid mechanics, Springer, Berlin, pp 215–471. http://link.springer.com/10.1007/978-3-540-30299-5_5

Meinders E, Hanjalic K (1999) Vortex structure and heat transfer in turbulent flow over a wall-mounted matrix of cubes. Int J Heat Fluid Flow 20:255–267

Nobach H (2016) A time-quantization based estimator for autocorrelation and spectral density estimation from laser Doppler anemometry data including local normalization. Tech. rep. http://nambis.bplaced.de/download/text/aquant.pdf

Nobach H, Müller E, Tropea C (1998) Efficient estimation of power spectral density from laser Doppler anemometer data. Exp Fluids 24(5):499–509. https://doi.org/10.1007/s003480050199

Oke TR (1988) Street design and urban canopy layer climate. Energy Build 11:103–113. https://doi.org/10.1016/0378-7788(88)90026-6

Perret L, Piquet T, Basley J, Mathis R (2017) Effects of plan area densities of cubical roughness elements on turbulent boundary layers. In: Congrès Français de Mécanique. https://cfm2017.sciencesconf.org/130816

Reynolds RT, Castro IP (2008) Measurements in an urban-type boundary layer. Exp Fluids 45(1):141–156. https://doi.org/10.1007/s00348-008-0470-z

Rivet C (2014) Etude en soufflerie atmosphérique des interactions entre canopée urbaine et basse atmosphère par PIV stéréoscopique. PhD thesis, Ecole Centrale de Nantes

Sakamoto H, Haniu H (1988) Aerodynamic forces acting on two square prisms placed vertically in a turbulent boundary layer. J Wind Eng Ind Aerodyn 31(1):41–66. http://www.sciencedirect.com/science/article/pii/0167610588901870

Savory E, Perret L, Rivet C (2013) Modeling considerations for examining the mean and unsteady flow in a simple urban-type street canyon. Meteorol Atmos Phys 121:1–16

Squire DT, Morrill-Winter C, Hutchins N, Schultz MP, Klewicki JC, Marusic I (2016) Comparison of turbulent boundary layers over smooth and rough surfaces up to high Reynolds numbers. J Fluid Mech 795:210–240. https://doi.org/10.1017/jfm.2016.196

Van Maanen HRE, Nobach H, Benedict Lv (1999) Improved estimator for the slotted autocorrelation function of randomly sampled LDA data. Meas Sci Technol 10(1):L4. https://doi.org/10.1088/0957-0233/10/1/002